Size dependance of the photo-induced phase transition in Ti_3O_5 nanocrystals

Ritwika Mandal

Jean Rouxel Institute of Materials, Nantes

Photoexcitation

- Photon absorption induces ***electronic excitation***
- The electron relaxes by imparting ***energy to the lattice system***; disruption of equilibrium position of atoms
- The vibration of atoms can be around their equilibrium position or resulting in overall shift of the equilibrium position

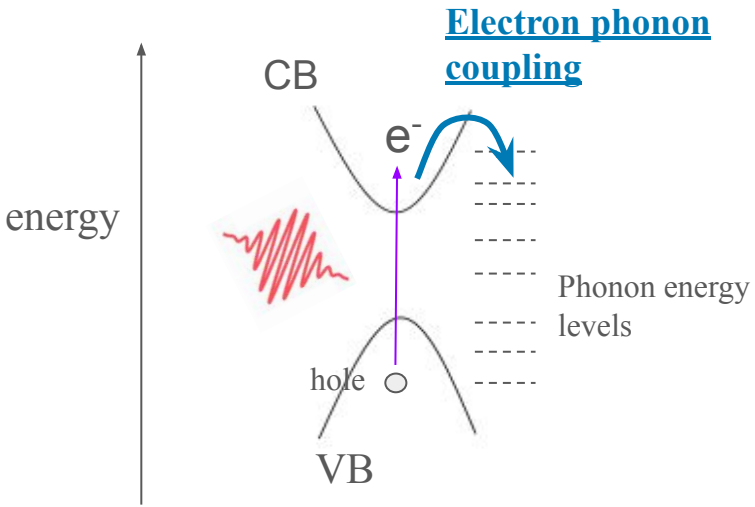

Photoexcitation

- Photon absorption induces ***electronic excitation***
- The electron relaxes by imparting ***energy to the lattice system***; disruption of equilibrium position of atoms
- The vibration of atoms can be around their equilibrium position or resulting in overall shift of the equilibrium position

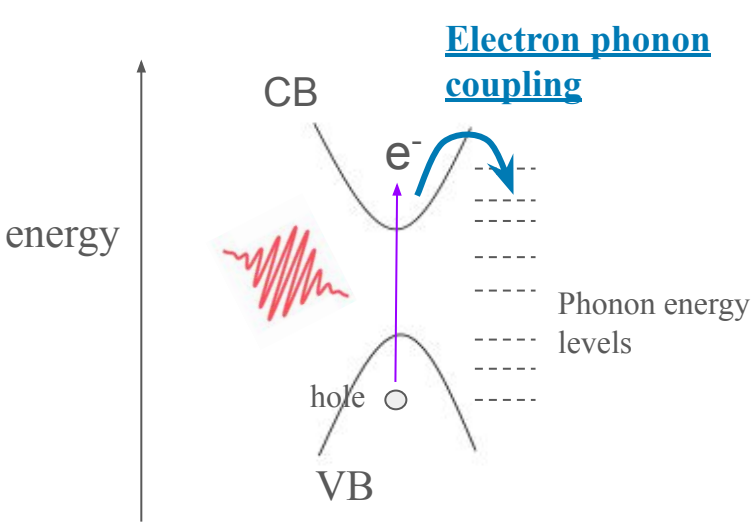

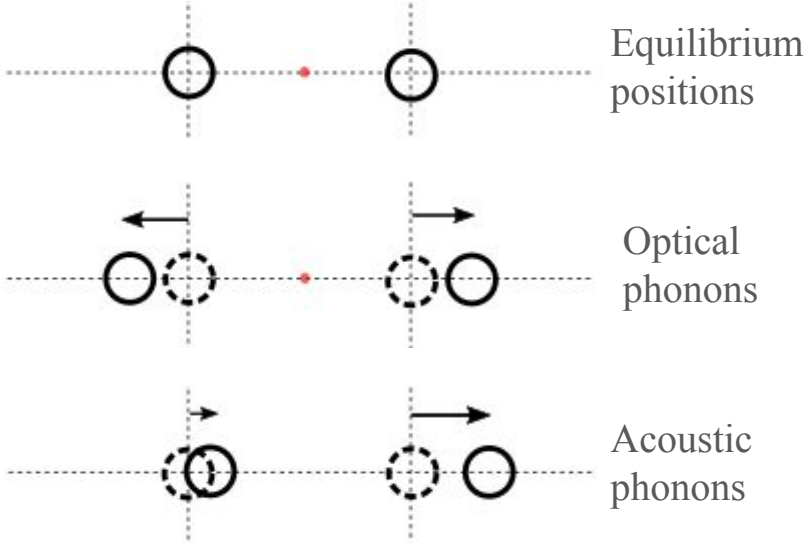

Boschetto, Davide & Rousse, Antoine. (2010). Coherent Optical Phonons in Bismuth Crystal. 10.5772/12901.

Multiscale dynamics

- Different subsystems unfold at different length and timescales
  - Electronic excitation immediately upon photoexcitation
  - Different phonon modes due to electron-phonon coupling
  - Thermal equilibrium governed by heat diffusion
  - Recovery of the system to its ground state (reversible changes)

- No master equation valid over all time scales

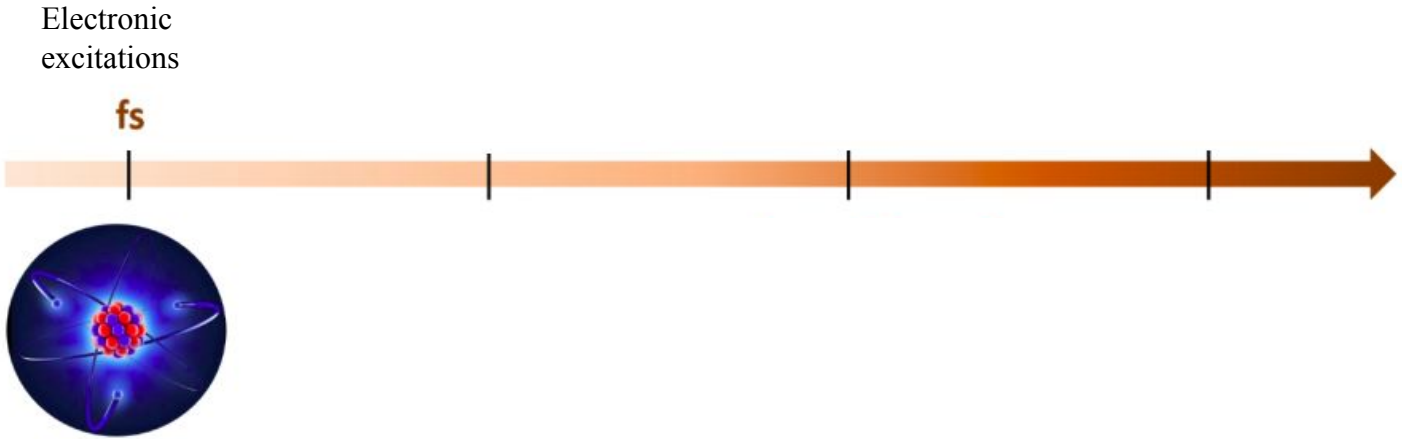

Multiscale dynamics

- Different subsystems unfold at different length and timescales
  - Electronic excitation immediately upon photoexcitation
  - Different phonon modes due to electron-phonon coupling
  - Thermal equilibrium governed by heat diffusion
  - Recovery of the system to its ground state (reversible changes)

- No master equation valid over all time scales

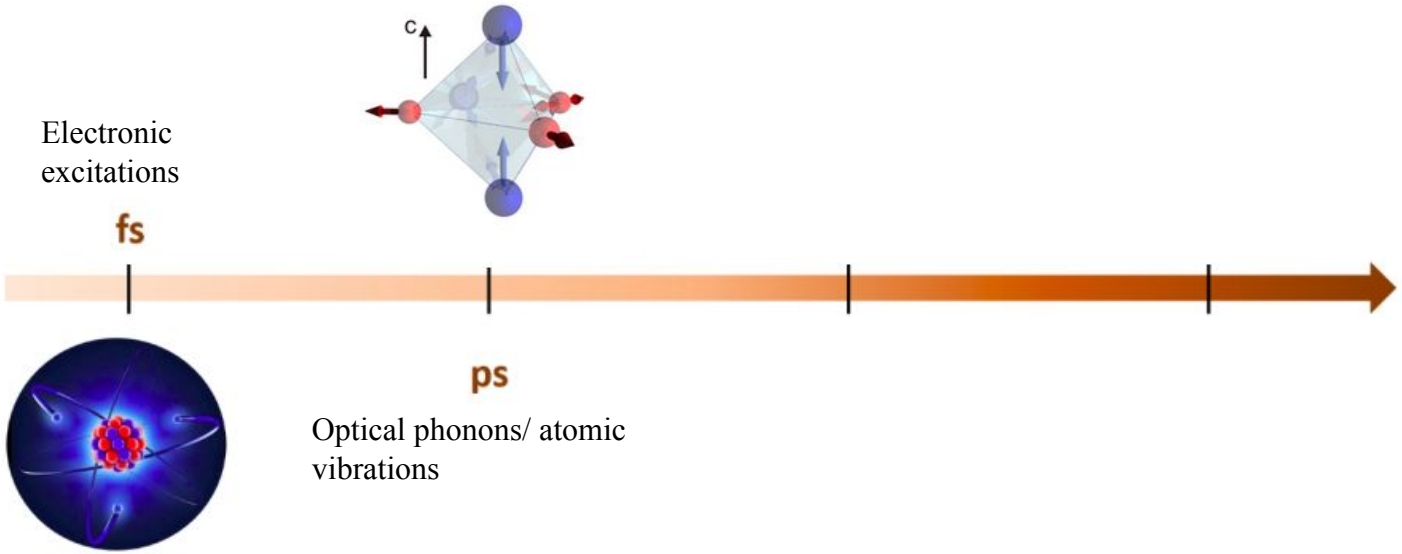

Multiscale dynamics

- Different subsystems unfold at different length and timescales
  - Electronic excitation immediately upon photoexcitation
  - Different phonon modes due to electron-phonon coupling
  - Thermal equilibrium governed by heat diffusion
  - Recovery of the system to its ground state (reversible changes)

- No master equation valid over all time scales

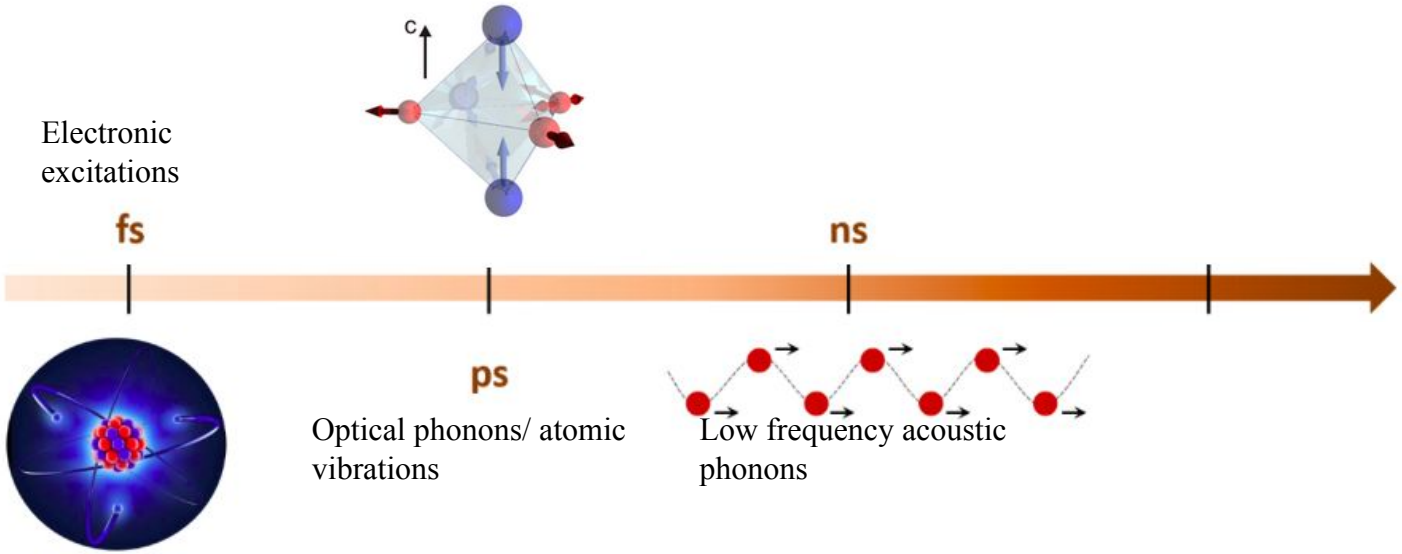

Multiscale dynamics

- Different subsystems unfold at different length and timescales
  - Electronic excitation immediately upon photoexcitation
  - Different phonon modes due to electron-phonon coupling
  - Thermal equilibrium governed by heat diffusion
  - Recovery of the system to its ground state (reversible changes)

- No master equation valid over all time scales

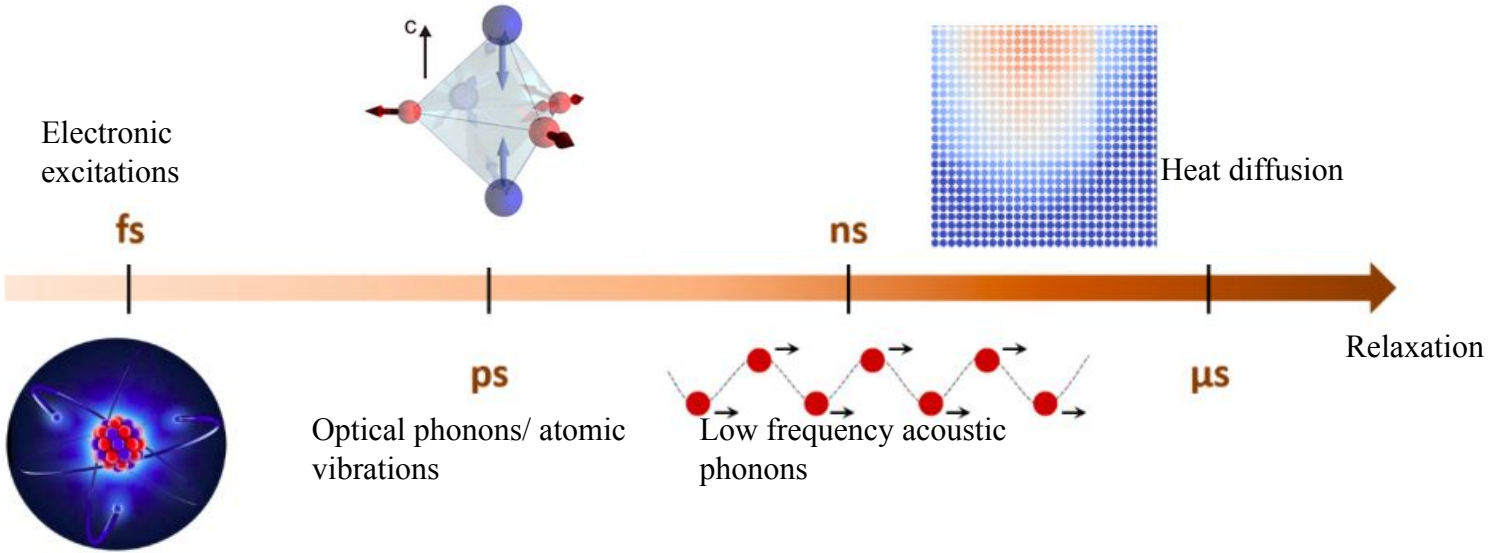

Phase transition upon photoexcitation

- The photo-excitation drives the system into a ***new energy landscape***
- It can drive the system transiently or permanently toward a ***new macroscopic state***
- This photo-induced macroscopic state can have a ***new lattice structure*** and/or ***electronic order***

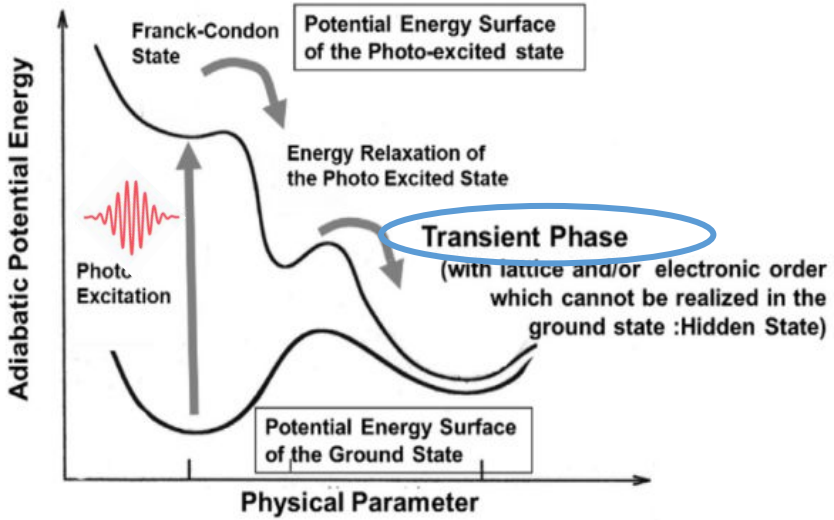

Nasu, K. (2004). Photoinduced phase transitions. World Scientific.

Semiconductor to metal phase transition in Ti_3O_5

- Semiconducting to metal transition at T ~ 460 K
- Transition is isostructural with an increase in volume of +6.4%

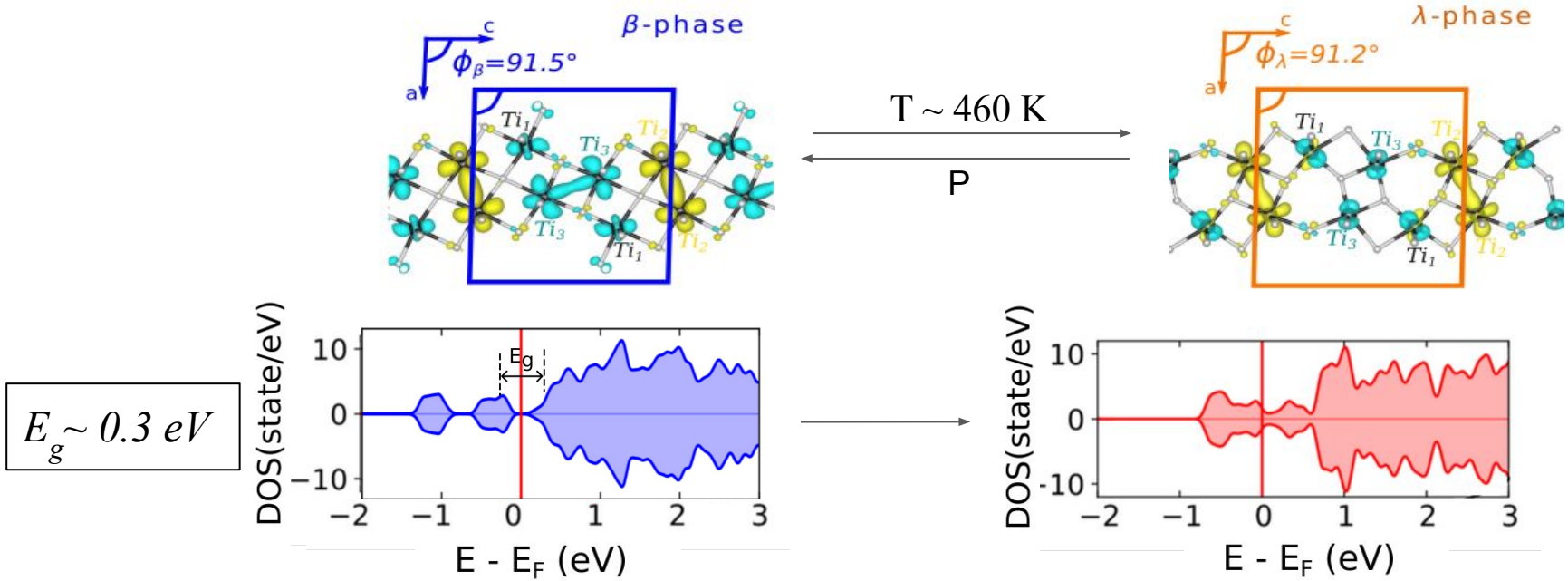

Onoda, M. "Phase transitions of Ti3O5." Journal of Solid State Chemistry 136.1 (1998): 67-73.

Semiconductor to metal phase transition in Ti_3O_5

We investigate the semiconductor to metal phase transition in Ti_3O_5 nanocrystals.

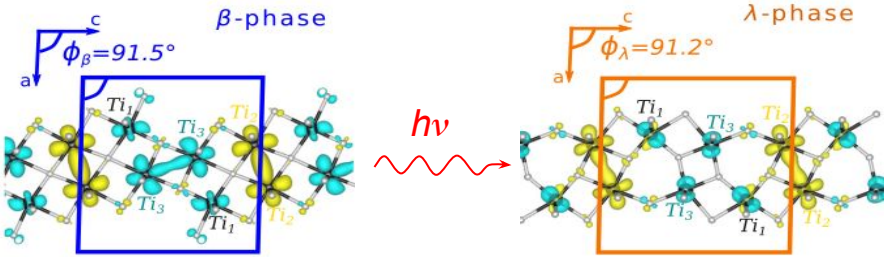

semiconducting metal

Semiconductor to metal phase transition in Ti_3O_5

We investigate the semiconductor to metal phase transition in Ti_3O_5 nanocrystals.

For ***nano-sized crystallites***, the metastable λ-phase is stable at room temperature, making the system ***bistable*** in a broad temperature range.

Great interest for technological applications (eg. heat storage, solar to steam generation)

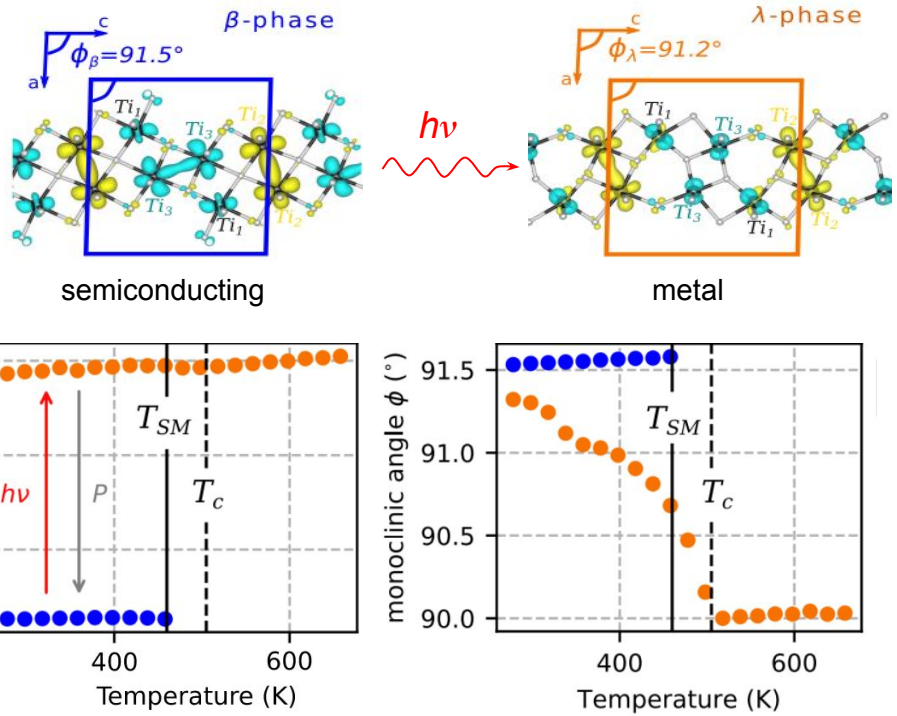

Yang, B., et al. Flatband λ-Ti_3O_5 towards extraordinary solar steam generation. Nature ***622****, 499–506 (2023).*
Tokoro et al. "External stimulation-controllable heat-storage ceramics." Nature communications 6.1 (2015): 1-8.
Ohkoshi, Shin-ichi, et al. "Low-pressure-responsive heat-storage ceramics for automobiles." Scientific reports 9.1 (2019): 1-8.

Semiconductor to metal phase transition in Ti_3O_5

We investigate the semiconductor to metal phase transition in Ti_3O_5 nanocrystals.

For ***nano-sized crystallites***, the metastable λ-phase is stable at room temperature, making the system ***bistable*** in a broad temperature range.

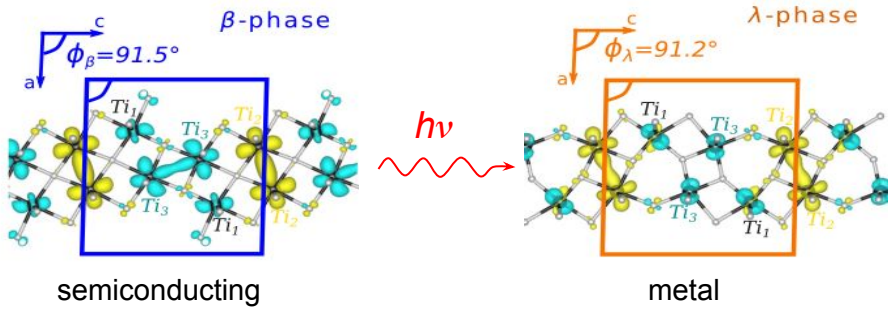

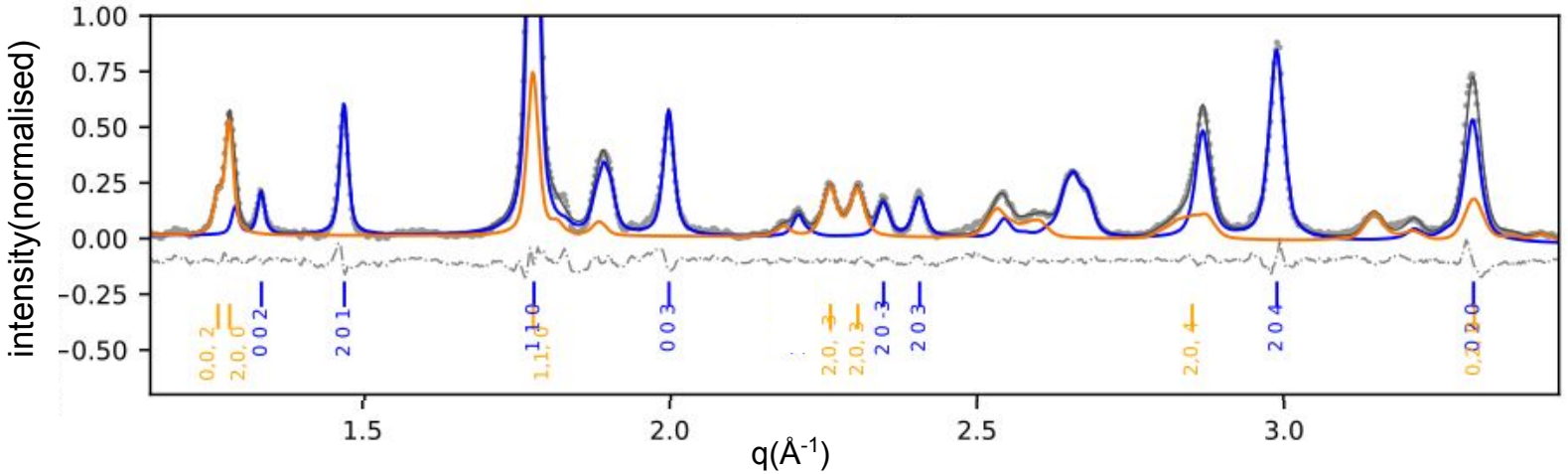

Photo-induced phase transition in Ti_3O_5 : State of the art

TR XRD measurement were performed on bistable Ti_3O_5 nanocrystal pellets with crystallite size 100 nm.

Dynamics showed ***phase front*** starting at the surface propagates in the bulk with ***sound velocity***.

Strain driven transformation

λ phase fraction

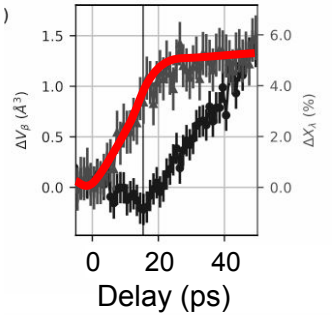

Unit cell volume

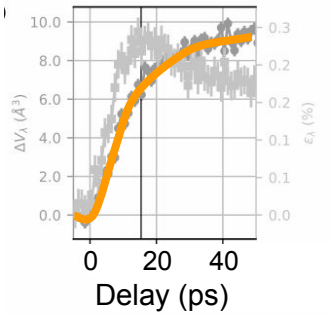

SwissFEL time scale (resolution 0.5ps)

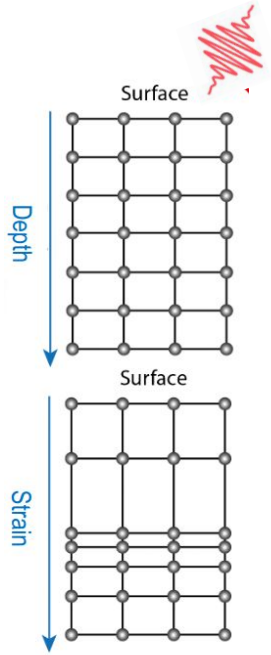

C. Mariette et al., Strain Wave Pathway to Semiconductor-to-Metal Transition revealed by time resolved X-ray powder diffraction, Nat Commun **12**, 1239 (2021)

Photo-induced phase transition in Ti_3O_5

TR XRD measurement were performed on bistable Ti_3O_5 nanocrystal pellets with crystallite size 100 nm.

Dynamics showed ***phase front*** starting at the surface propagates in the bulk with ***sound velocity***.

Strain driven transformation

λ phase fraction

Unit cell volume

SwissFEL time scale (resolution 0.5ps)

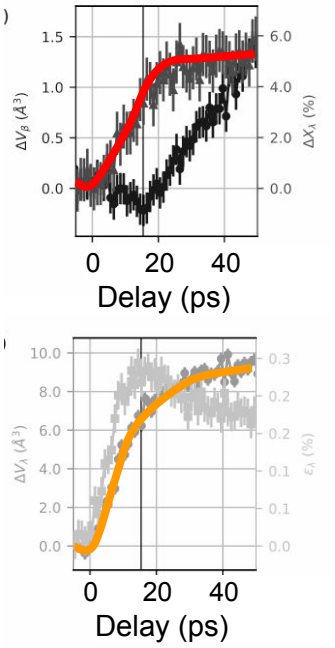

Strainwave driven transformation

Thermal transformation/ Heat diffusion

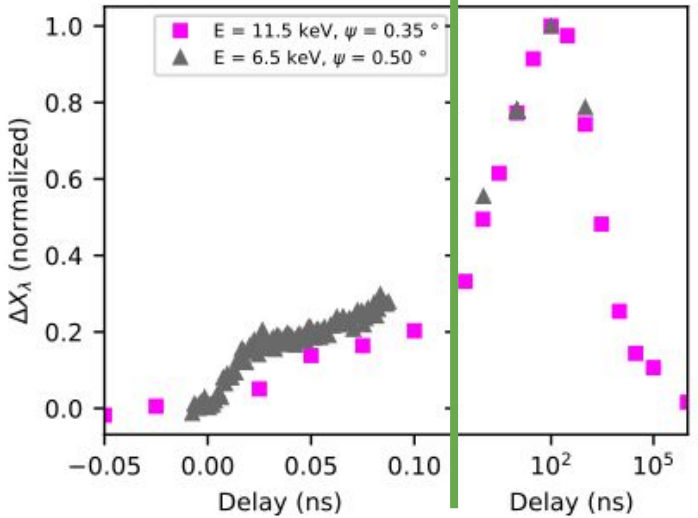

ESRF time scale (resolution 100ps)

C. Mariette et al., Strain Wave Pathway to Semiconductor-to-Metal Transition revealed by time resolved X-ray powder diffraction, Nat Commun **12**, 1239 (2021)

Photo-induced phase transition in Ti_3O_5

TR XRD measurement were performed on bistable Ti_3O_5 nanocrystal pellets with crystallite size 100 nm.

Dynamics showed ***phase front*** starting at the surface propagates in the bulk with ***sound velocity***.

Strain driven transformation

λ phase fraction

Unit cell volume

SwissFEL time scale (resolution 0.5ps)

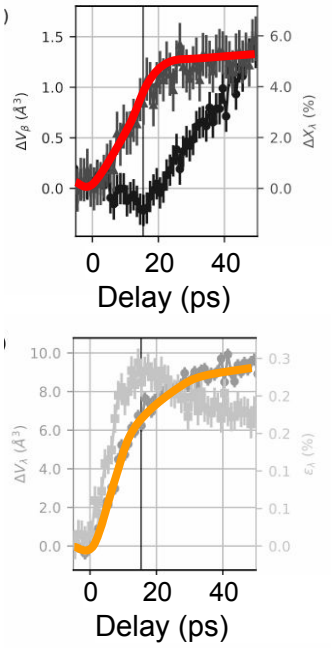

Strainwave driven transformation

Thermal transformation/ Heat diffusion

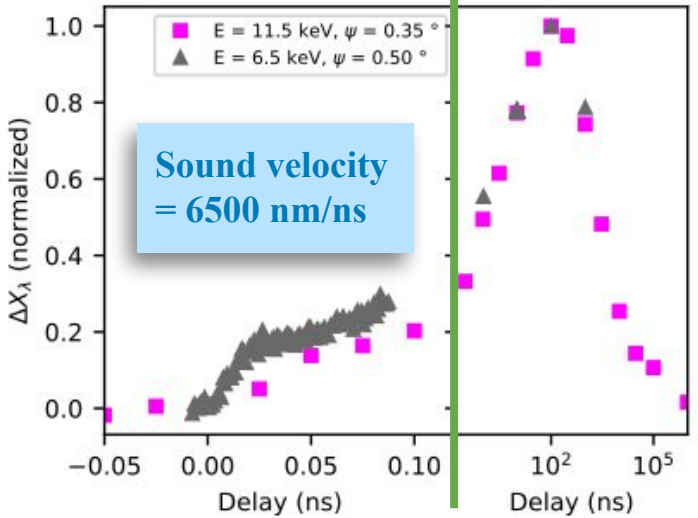

ESRF time scale (resolution 100ps)

C. Mariette et al., Strain Wave Pathway to Semiconductor-to-Metal Transition revealed by time resolved X-ray powder diffraction, Nat Commun **12**, 1239 (2021)

Photo-induced phase transition in Ti_3O_5

TR XRD measurement were performed on bistable Ti_3O_5 nanocrystal pellets with crystallite size 100 nm.

Dynamics showed ***phase front*** starting at the surface propagates in the bulk with ***sound velocity***.

Strain driven transformation

λ phase fraction

Unit cell volume

SwissFEL time scale (resolution 0.5ps)

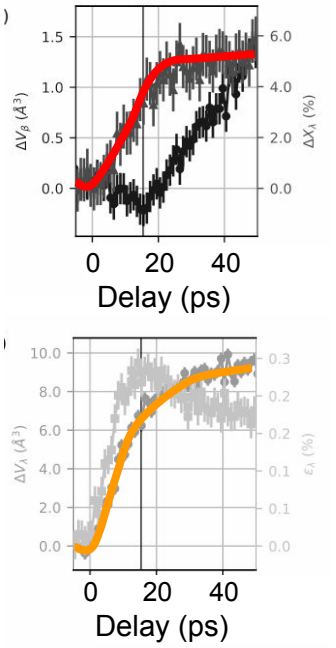

Strainwave driven transformation

Thermal transformation/ Heat diffusion

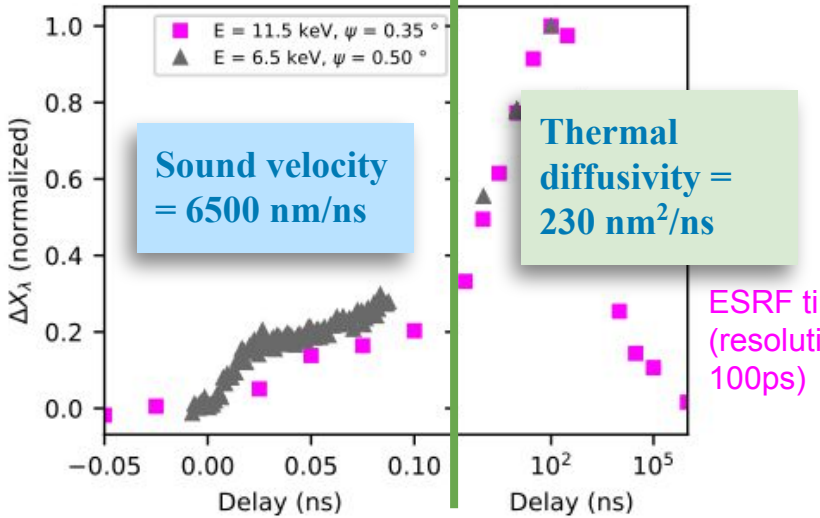

Sound velocity = 6500 nm/ns

Thermal diffusivity = 230 nm^2/ns

ESRF time scale (resolution 100ps)

C. Mariette et al., Strain Wave Pathway to Semiconductor-to-Metal Transition revealed by time resolved X-ray powder diffraction, Nat Commun **12**, 1239 (2021)

Open questions

Previous observations:

- 30% crystallites transformed within the first layer
- ***optical anisotropy*** of the randomly oriented crystallites in the pellet
- transition is favoured when ***pump pulse is along ab plane***

A. Asahara, et.al, Phys. Rev. B 90, 014303/1-7 (2014).
Saiki T, et.al, Phys. Rev. B 105, 075134
C. Mariette et al., Nat Comm. 2021

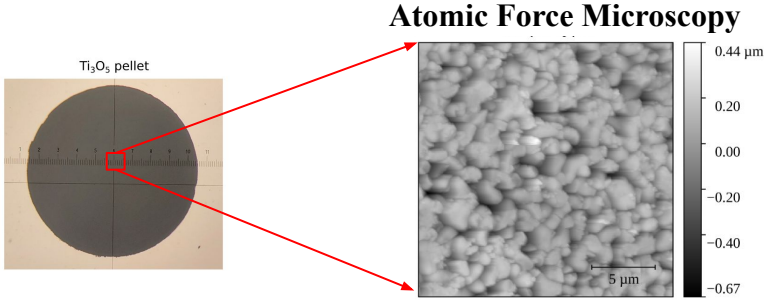

Previous Hypothesis:

All crystallites with favourable orientation are fully transformed (⅓),
The crystallites with unfavourable orientation are not transformed

Open questions

Previous observations:

- 30% crystallites transformed within the first layer
- ***optical anisotropy*** of the randomly oriented crystallites in the pellet
- transition is favoured when ***pump pulse is along ab plane***

A. Asahara, et.al, Phys. Rev. B 90, 014303/1-7 (2014).
Saiki T, et.al, Phys. Rev. B 105, 075134
C. Mariette et al., Nat Comm. 2021

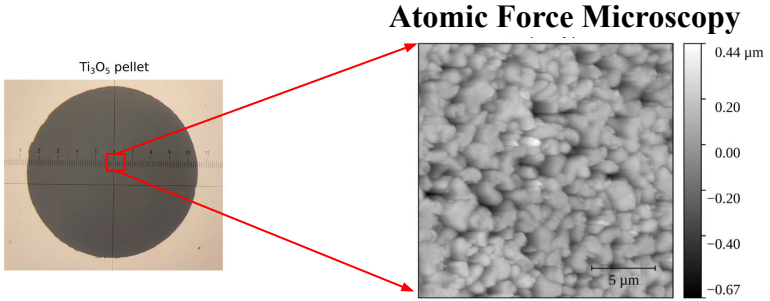

Previous Hypothesis:

All crystallites with favourable orientation are fully transformed (⅓),
The crystallites with unfavourable orientation are not transformed

What is the ***effect of morphology on the efficiency and timescales*** of photoinduced phase transitions in Ti_3O_5 nanocrystals?

Open questions

λ and β Ti_3O_5 with different crystallite size have been synthesized by our collaborators in Tokyo University
(S.-I. Ohkoshi, Marie Yoshikiyo and Hiroko Tokoro)

flake-type

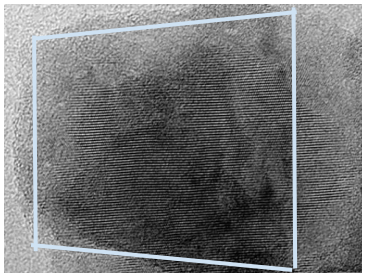

stripe-type

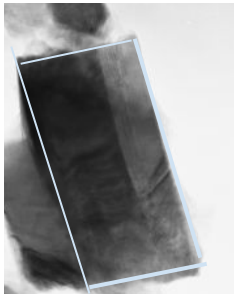

block-type

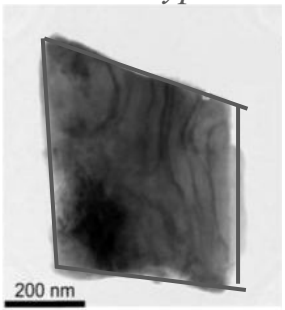

Dimension of crystallites: < 100 nm [1] | 200 nm X 100 nm [2] | 500 nm [3]

The three morphologies have similar transition temperature but different transition pressure

1] Ohkoshi, Shin-ichi, et al. "Synthesis of a metal oxide with a room-temperature photoreversible phase transition." Nature chemistry 2.7 (2010): 539.
[2] Tokoro, Hiroko, et al. "External stimulation-controllable heat-storage ceramics." Nature communications 6.1 (2015): 1-8.
[3] Ohkoshi, Shin-ichi, et al. "Low-pressure-responsive heat-storage ceramics for automobiles." Scientific reports 9.1 (2019): 1-8.

Time resolved X-ray diffraction

- **Ultrashort** laser pulse (pump) ~ 1 ps incident normal
- **Ultrashort** X-ray pulse (probe) ~ 100 ps
- Synchronized in time
- Diffraction at near grazing angle to probe only the laser-excited surface.

Laser penetration depth ~ **70 nm**
X-ray penetration depth ~ 450 nm at 0.4^0 incidence angle

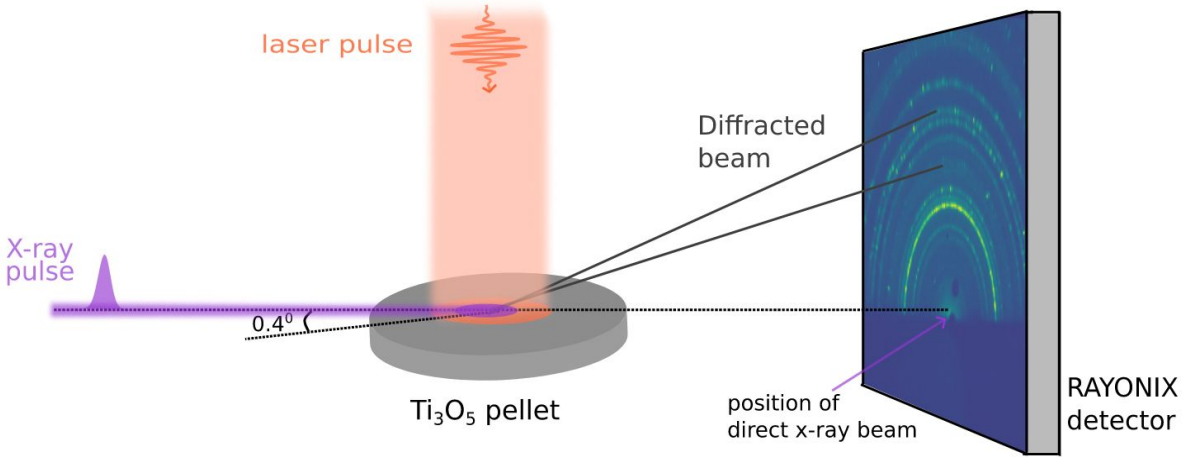

Time resolved X-ray diffraction

- **Ultrashort** laser pulse (pump) ~ 1 ps incident normal
- **Ultrashort** X-ray pulse (probe) ~ 100 ps
- Synchronized in time
- Diffraction at near grazing angle to probe only the laser-excited surface.

Laser penetration depth ~ **70 nm**
X-ray penetration depth ~ 450 nm at 0.4^0 incidence angle

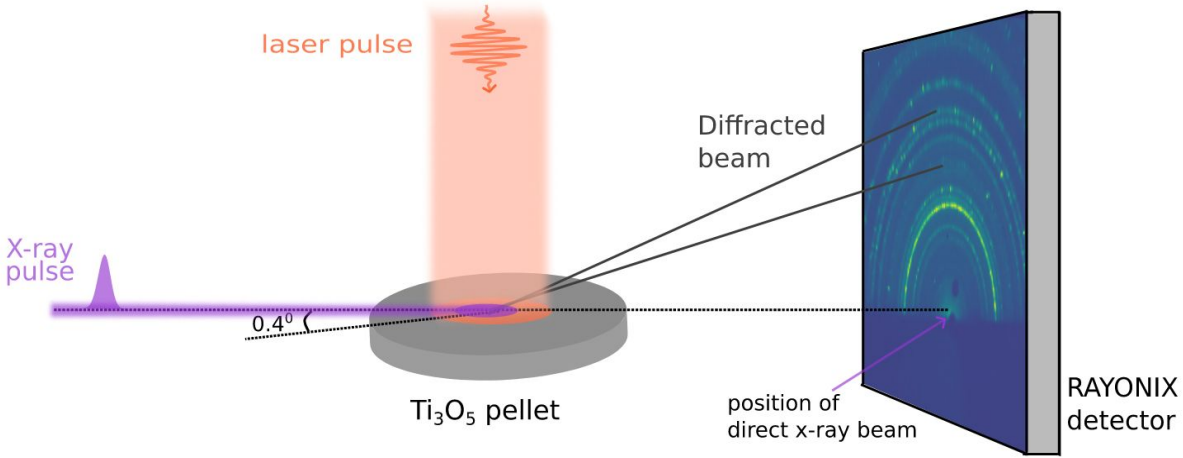

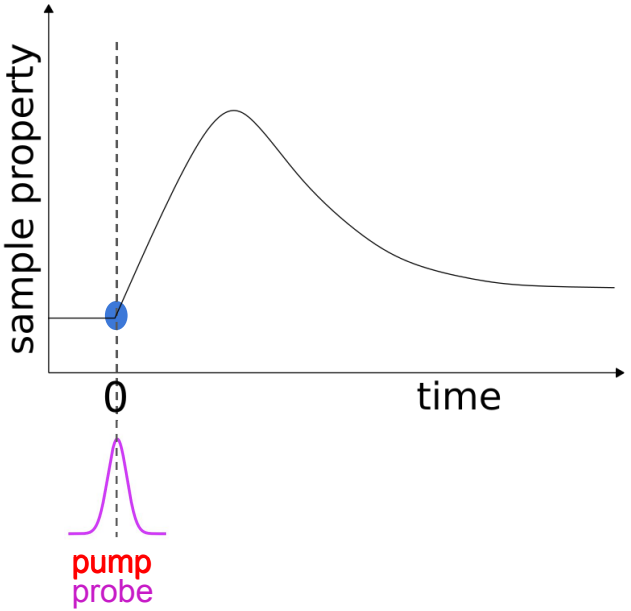

Time resolved X-ray diffraction

- **Ultrashort** laser pulse (pump) ~ 1 ps incident normal
- **Ultrashort** X-ray pulse (probe) ~ 100 ps
- Synchronized in time
- Diffraction at near grazing angle to probe only the laser-excited surface.

Laser penetration depth ~ **70 nm**
X-ray penetration depth ~ 450 nm at 0.4^0 incidence angle

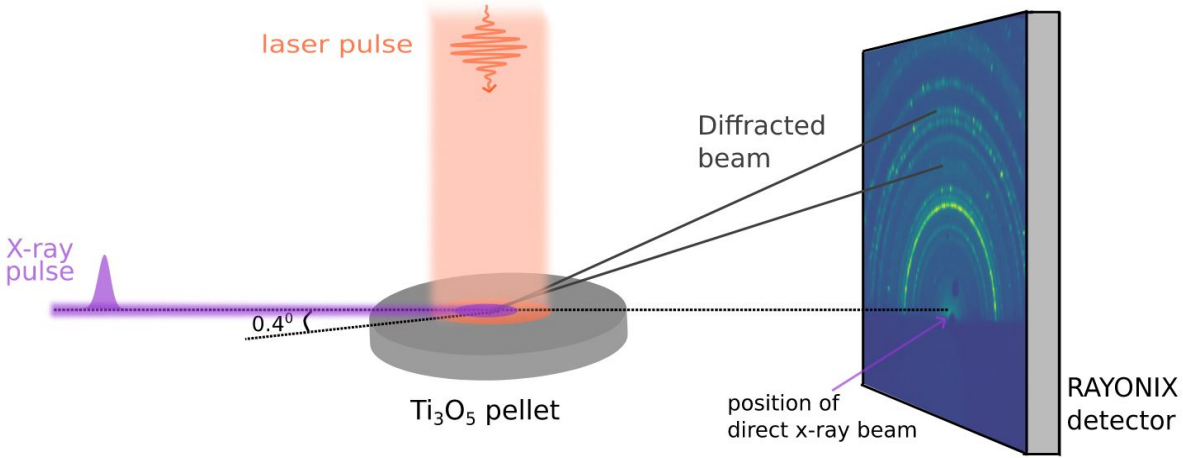

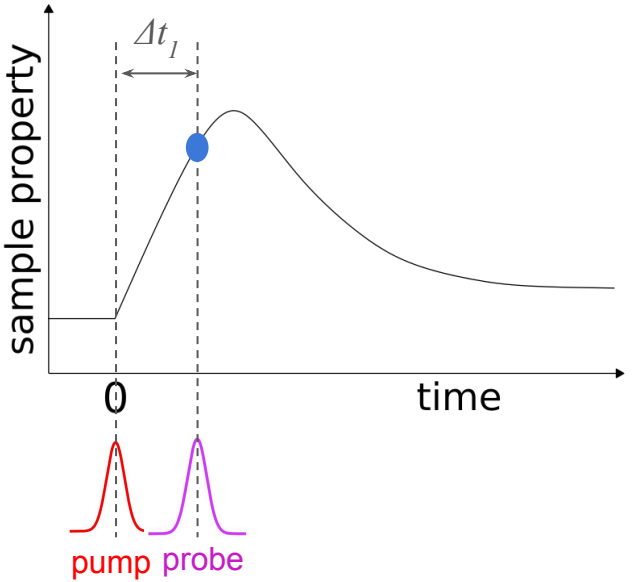

Time resolved X-ray diffraction

- **Ultrashort** laser pulse (pump) ~ 1 ps incident normal
- **Ultrashort** X-ray pulse (probe) ~ 100 ps
- Synchronized in time
- Diffraction at near grazing angle to probe only the laser-excited surface.

Laser penetration depth ~ **70 nm**
X-ray penetration depth ~ 450 nm at 0.4^0 incidence angle

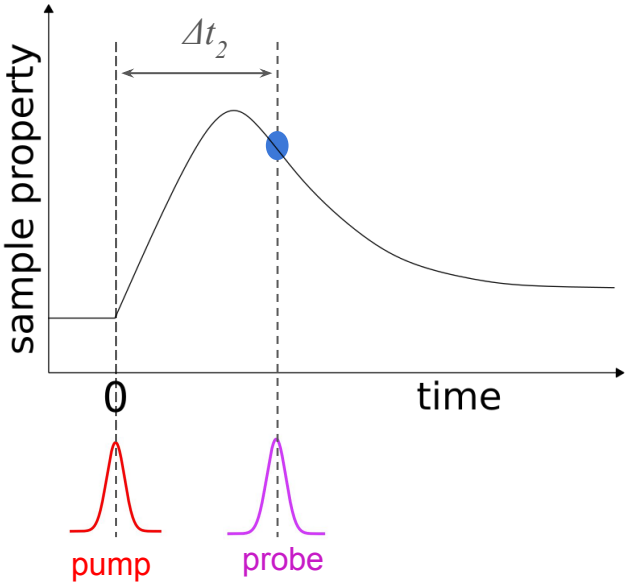

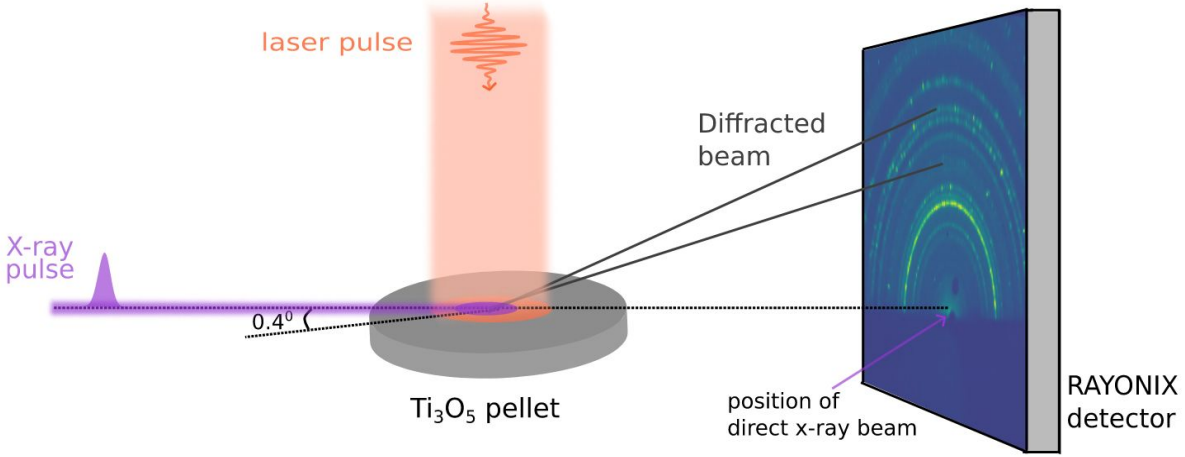

Time resolved X-ray diffraction

- **Ultrashort** laser pulse (pump) ~ 1 ps incident normal
- **Ultrashort** X-ray pulse (probe) ~ 100 ps
- Synchronized in time
- Diffraction at near grazing angle to probe only the laser-excited surface.

Laser penetration depth ~ **70 nm**
X-ray penetration depth ~ 450 nm at 0.4^0 incidence angle

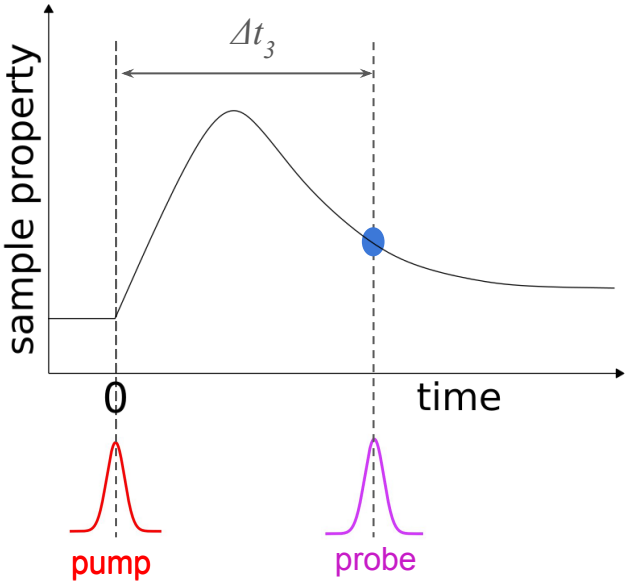

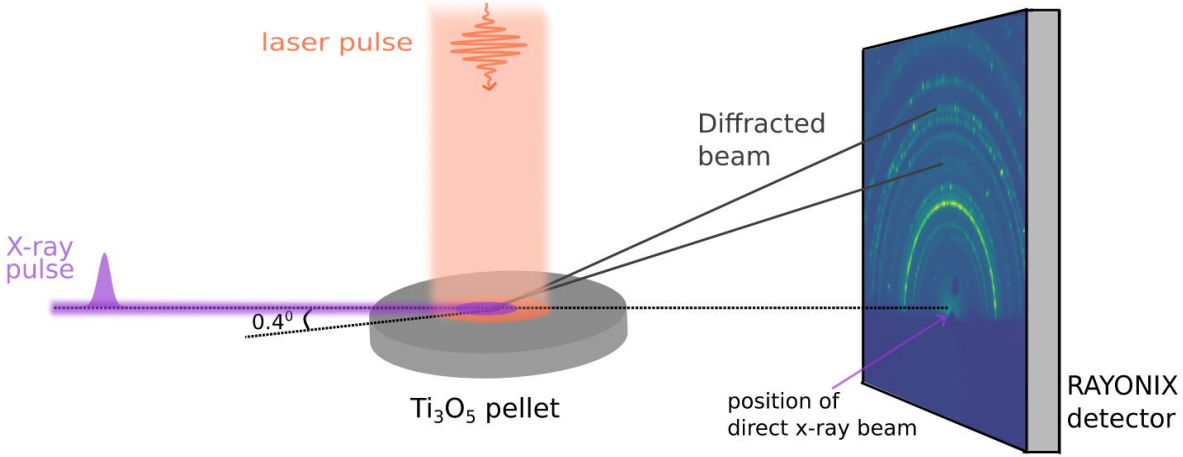

Time resolved X-ray diffraction

- **Ultrashort** laser pulse (pump) ~ 1 ps incident normal
- **Ultrashort** X-ray pulse (probe) ~ 100 ps
- Synchronized in time
- Diffraction at near grazing angle to probe only the laser-excited surface.

Laser penetration depth ~ **70 nm**
X-ray penetration depth ~ 450 nm at 0.4^0 incidence angle

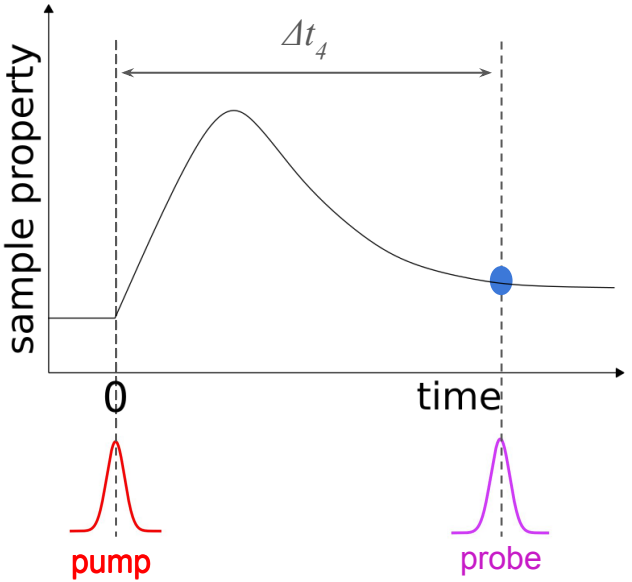

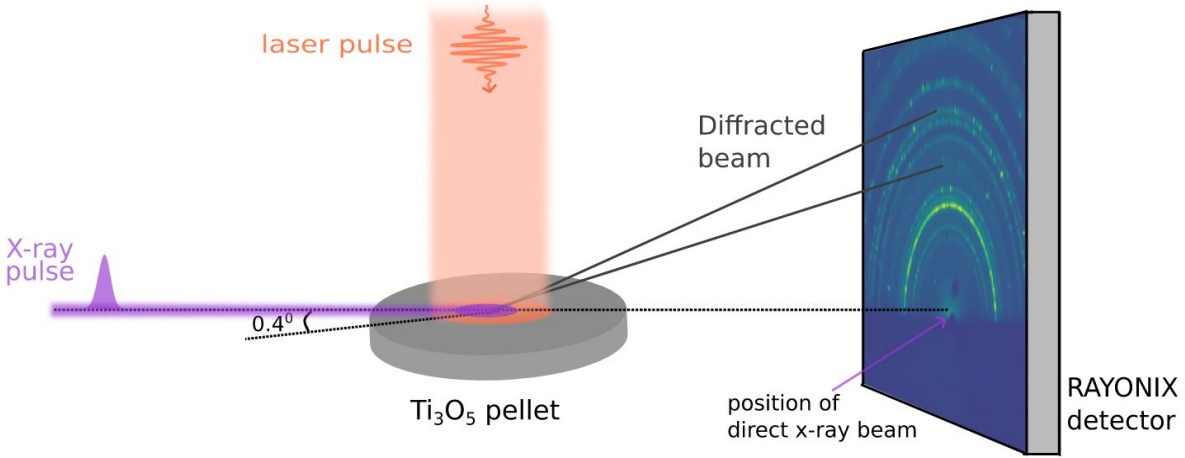

Time resolved X-ray diffraction

- **Ultrashort** laser pulse (pump) ~ 1 ps incident normal
- **Ultrashort** X-ray pulse (probe) ~ 100 ps
- Synchronized in time
- Diffraction at near grazing angle to probe only the laser-excited surface.

Laser penetration depth ~ **70 nm**
X-ray penetration depth ~ 450 nm at 0.4^0 incidence angle

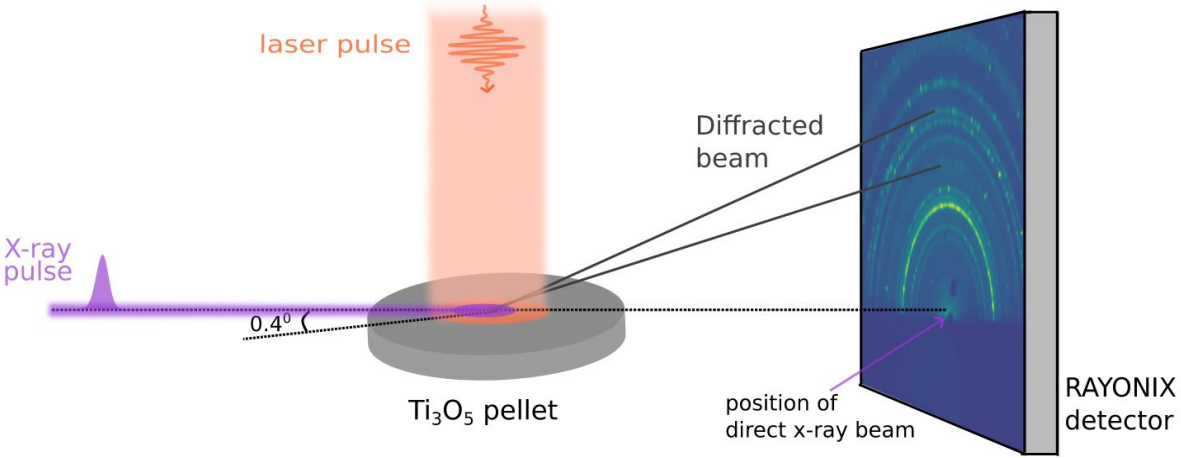

ESRF(**European Synchrotron Radiation Facility**)

Time resolved X-ray diffraction

- A set of time delays with interleaved off/negative delay (reference pattern)
- The sequence of time delays (below eg. 30 delays) is repeated several times (below eg. 4 times) to increase the statistics and track experimental drifts.

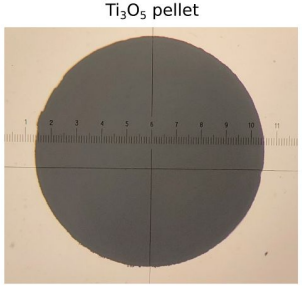

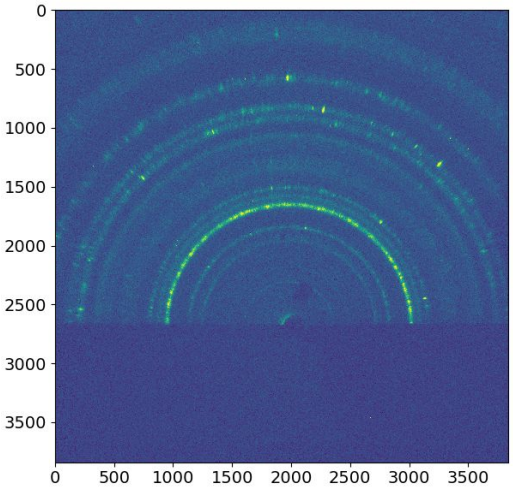

Time resolved X-ray diffraction

- A set of time delays with interleaved off/negative delay (reference pattern)
- The sequence of time delays (below eg. 30 delays) is repeated several times (below eg. 4 times) to increase the statistics and track experimental drifts.

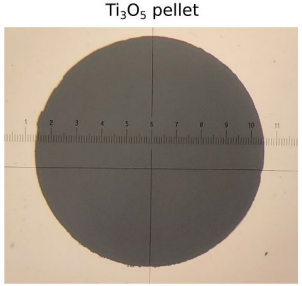

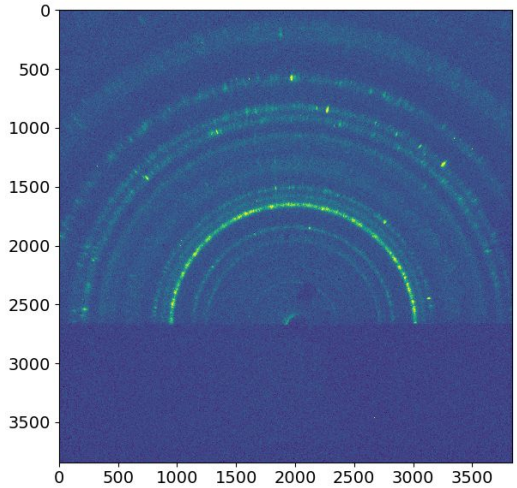

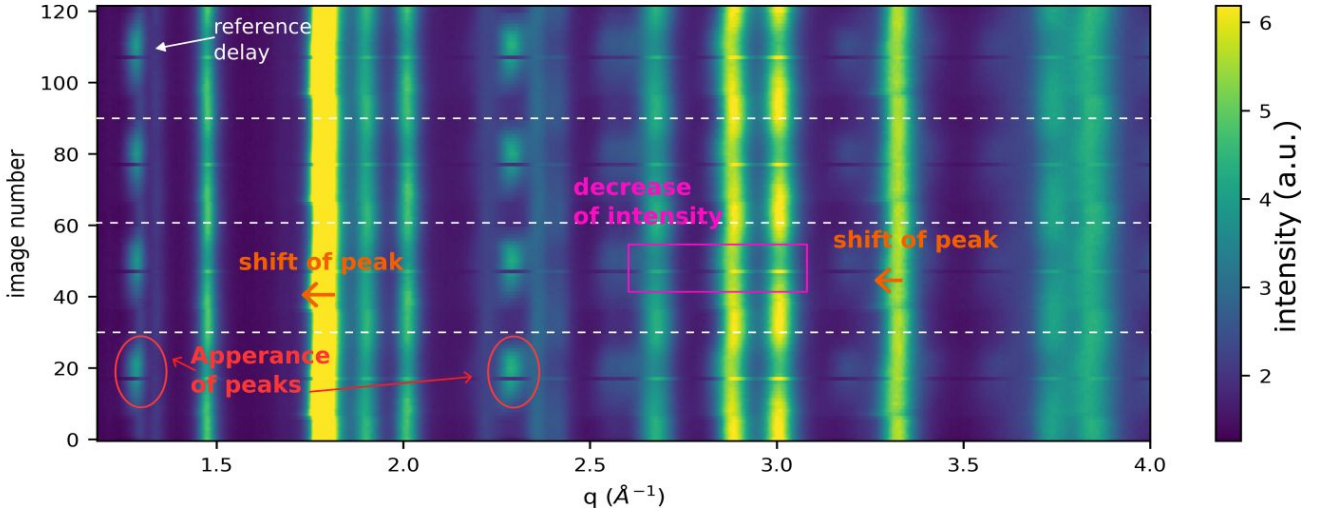

Diffraction patterns at different delays

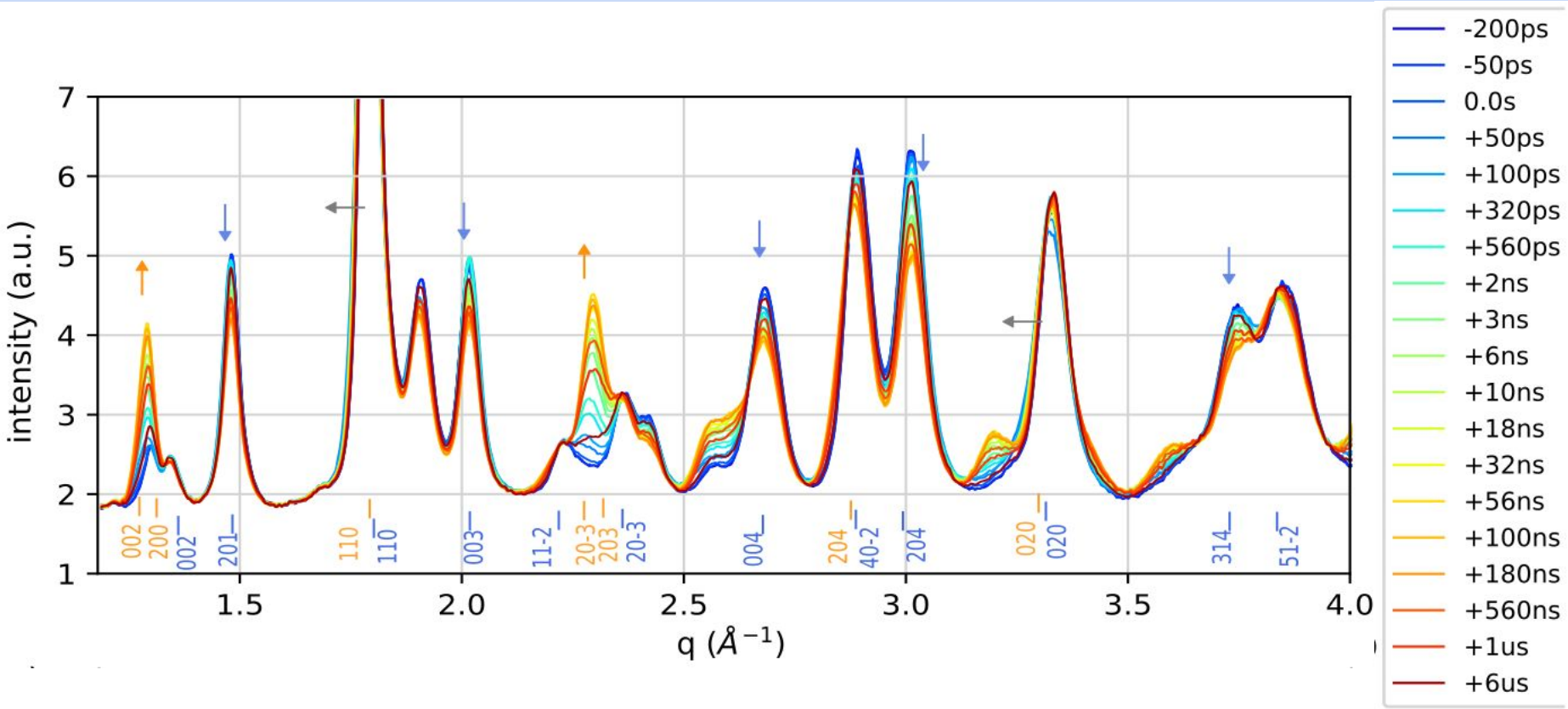

Observations from the comparison plots:

Whole dynamics:

Rietveld refinement allowed us to retrieve temporal evolution of the λ phase fraction.

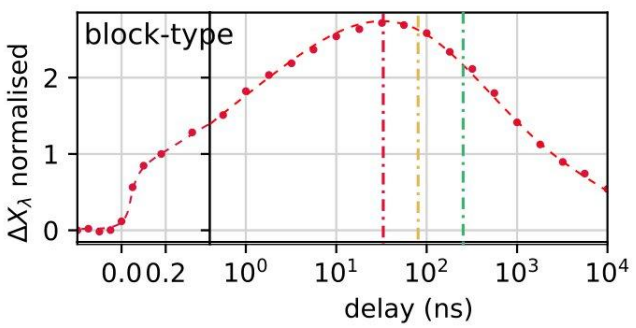

Observations from the comparison plots:

Characterisation of phase transition dynamics with various crystallite sizes

Other parameters are kept same:

- laser fluence = 0.5 mJ/mm^2
- Incidence angle of x-ray beam = 0.4°
- Laser wavelength = 800 nm

Peak of the ΔX_λ occurs at different delays for:

Flake-type: 200 ns
Stripe-type: 65 ns
Block-type: 38 ns

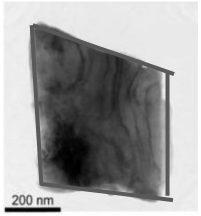

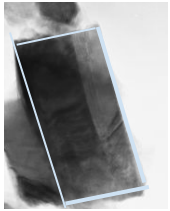

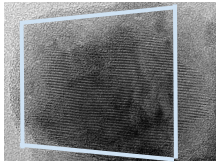

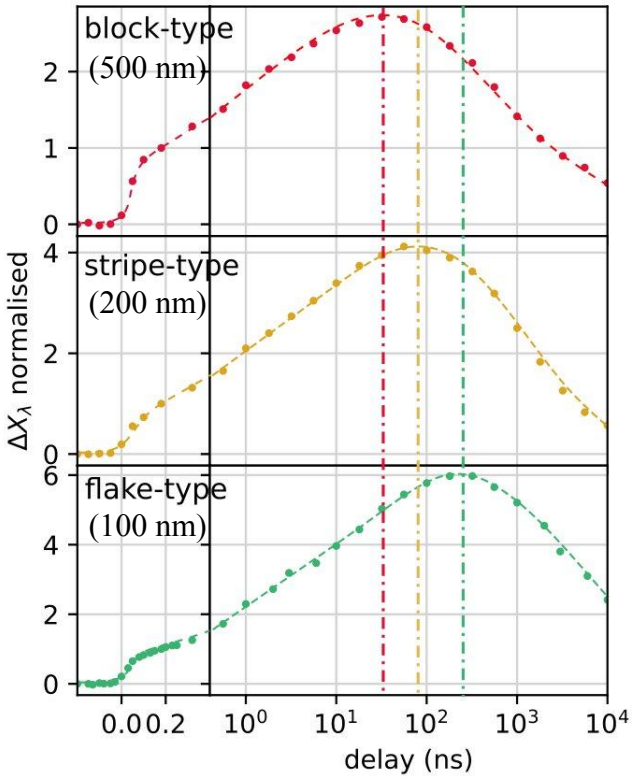

Heat diffusion peak of phase transformation ***occurs earlier for the bigger crystallites***

Results and observation from the comparison plots:

Influence of incident laser fluence on the phase transition dynamics

Linear dependence on the laser fluence at 200 ps (transformed by strainwave)
Non-linear dependence with fluence at 100 ns (transformed by heat diffusion)

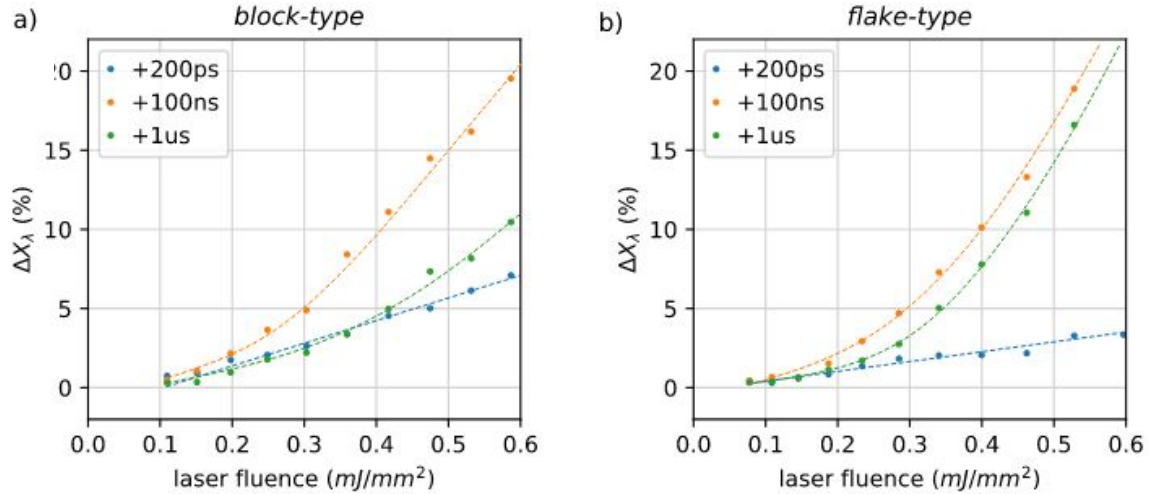

Different fluence dependencies confirm the ***different mechanism at play on 200 ps and 100 ns time scales***

Model simulations

- Finite difference method
- Heat flux is calculated at each node and each time step
- Three different heat exchange coefficients - intragrain, intergrain and with the surrounding
- At each time step, the temperature of each node is calculated and based on it the phase of node is checked

In collaboration with L Stoleriu & C Enachescu, University of Iasi

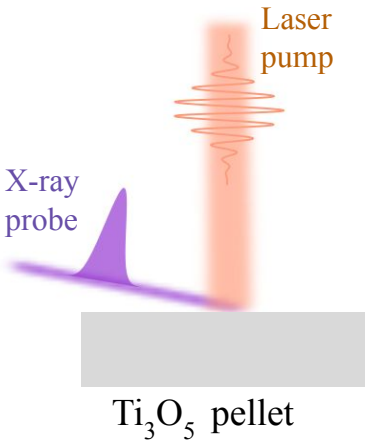

Model simulations

- Finite difference method
- Heat flux is calculated at each node and each time step
- Three different heat exchange coefficients - intragrain, intergrain and with the surrounding
- At each time step, the temperature of each node is calculated and based on it the phase of node is checked

In collaboration with L Stoleriu & C Enachescu, University of Iasi

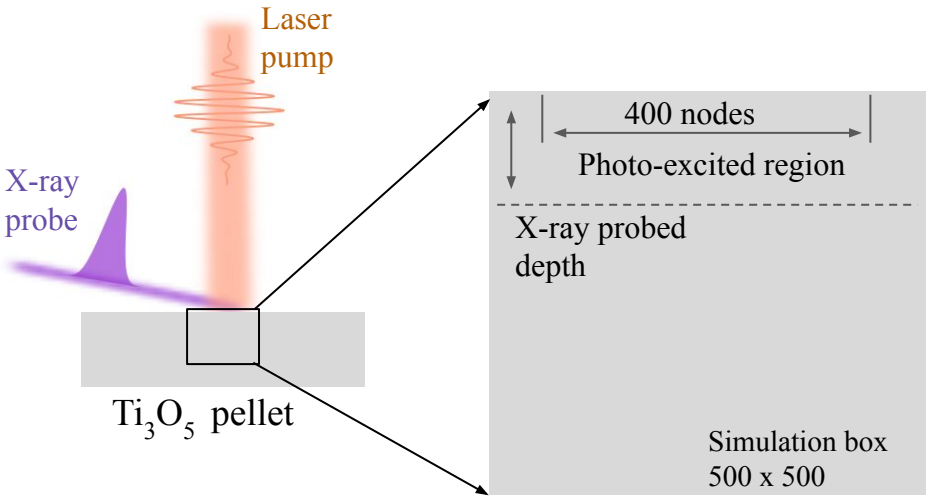

Model simulations

- Finite difference method
- Heat flux is calculated at each node and each time step
- ***Three different heat exchange coefficients*** - intragrain, intergrain and with the surrounding
- At each time step, the ***temperature*** of each node is calculated and based on it the ***phase*** of node is checked

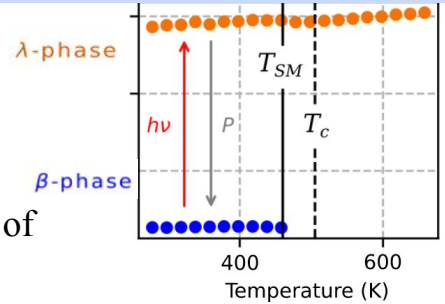

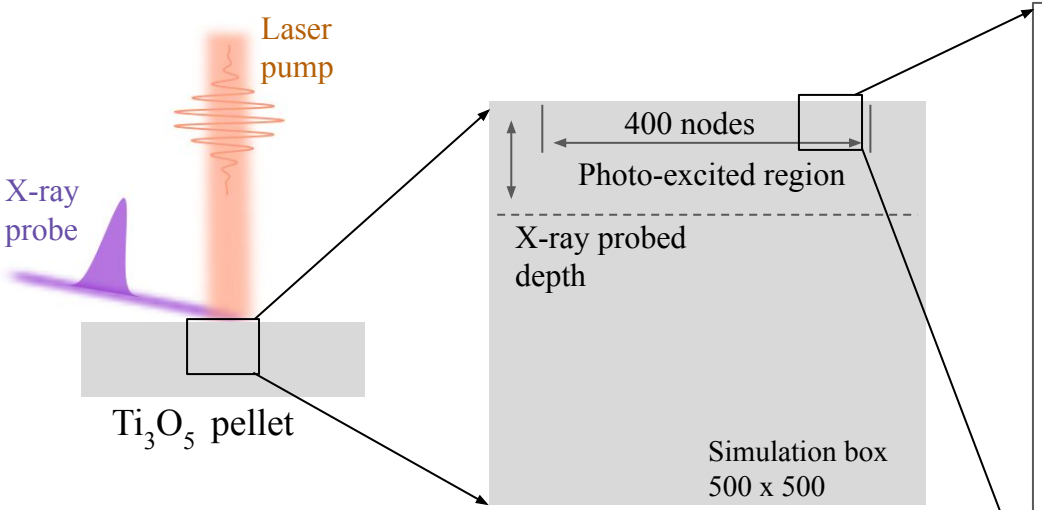

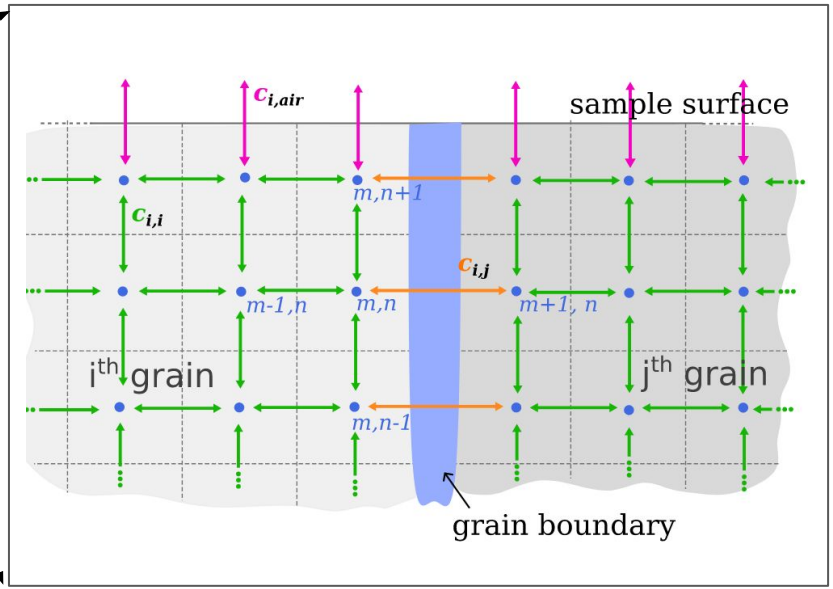

Open questions

Previous observations:

- Maximum of 30% crystallites transformed within the first layer
- ***optical anisotropy*** of the randomly oriented crystallites in the pellet
- transition is favoured when ***pump pulse is along ab plane***

A. Asahara, et.al, Phys. Rev. B 90, 014303/1-7 (2014).
Saiki T, et.al, Phys. Rev. B 105, 075134
C. Mariette et al., Nat Comm. 2021

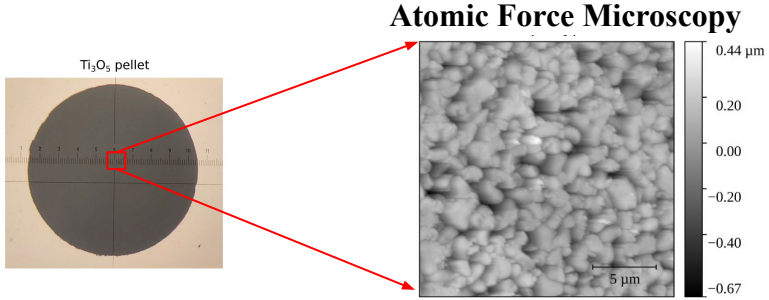

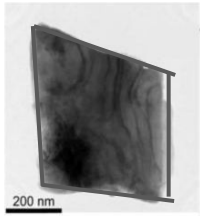

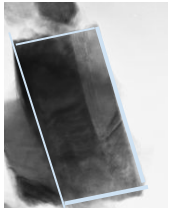

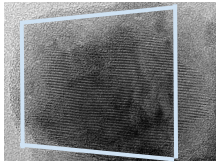

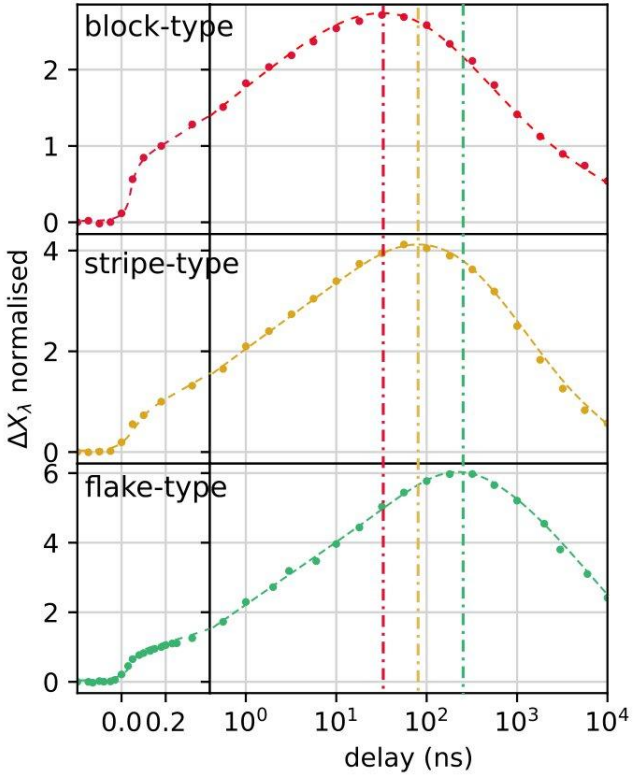

Excitation of the whole grain within the first layer

Initial state: λ-phase domains that are whole crystallites on the photo-excited surface

~ ⅓ rd of the crystallites on the surface are in λ phase

Grainsize: 10x10

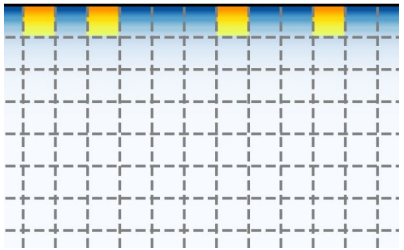

Grainsize: 20x20

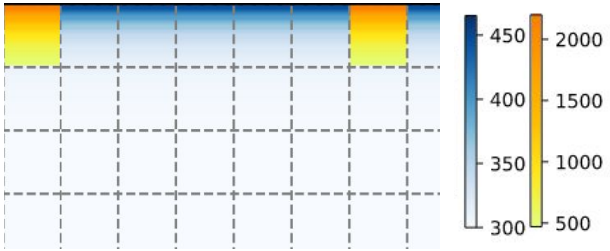

Excitation of the whole grain within the first layer

Initial state: λ-phase domains that are whole crystallites on the photo-excited surface

~ ⅓ rd of the crystallites on the surface are in λ phase

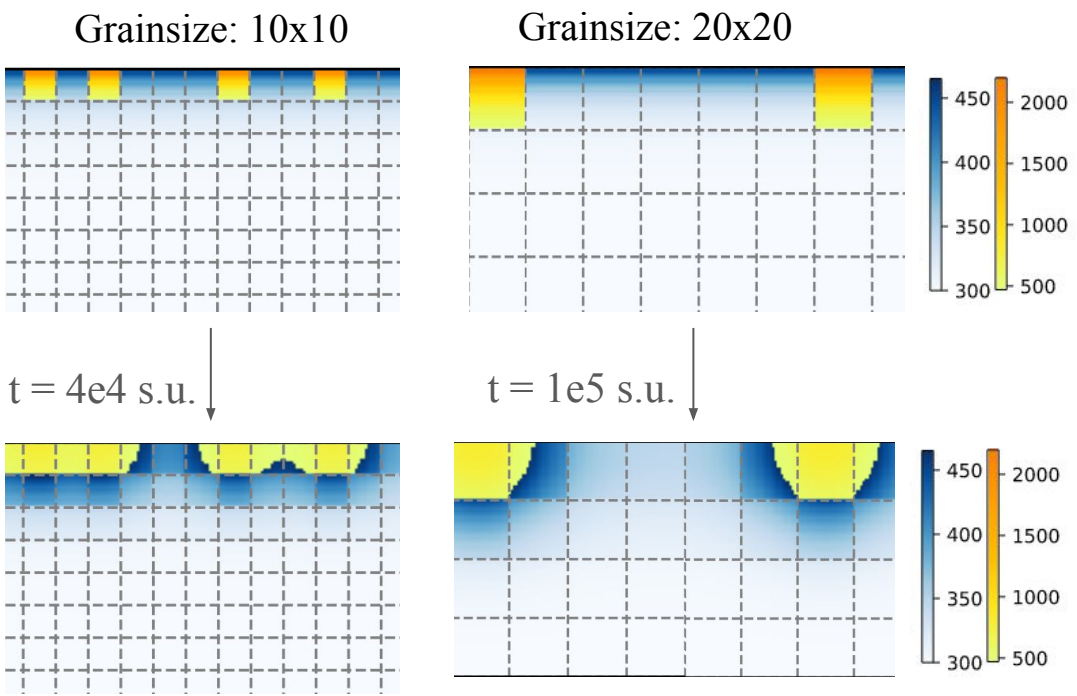

Excitation of the whole grain within the first layer

Initial state: λ-phase domains that are whole crystallites on the photo-excited surface

~ ⅓ rd of the crystallites on the surface are in λ phase

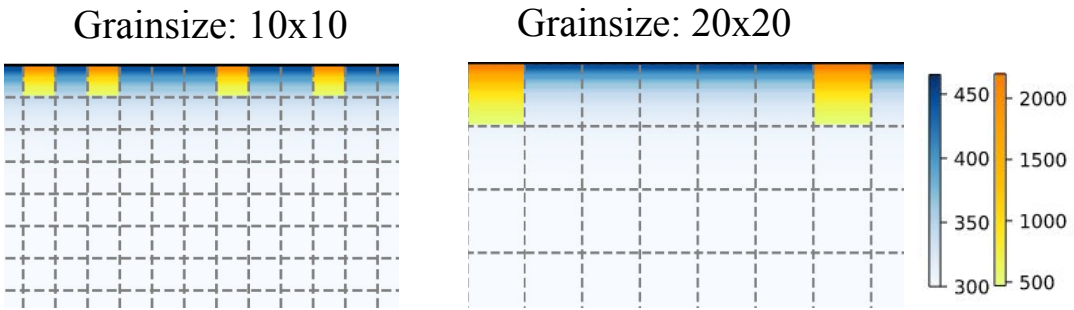

- Difference in the peak position for the two systems; in opposite trend to the experimental results(Irrespective of the inter- and intra-grain coefficients)

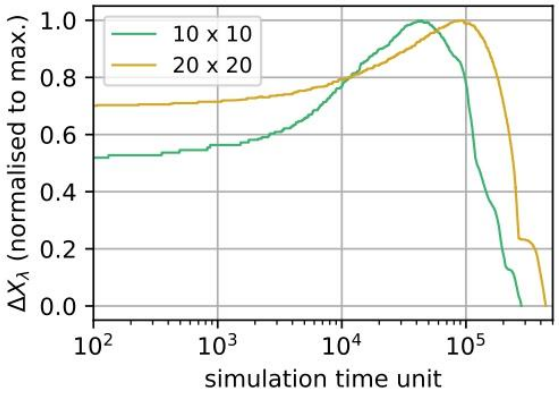

Whole grain transformation cannot explain the size dependance in the ns dynamics.

Phase separation on surface and extends in depth in the bigger grain

Initial state: λ-phase domains that show

1. phase separation within a crystallite
2. Extending in depth in the bigger crystallites

Grainsize: 10x10

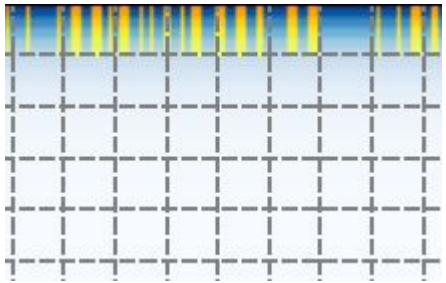

Grainsize: 50x50

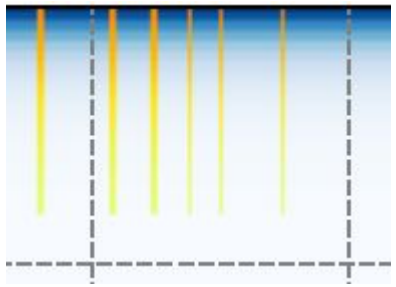

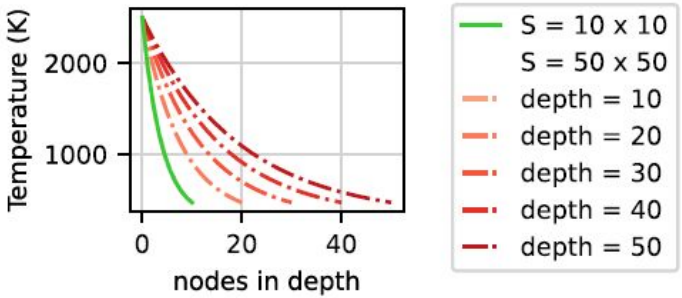

Phase separation on surface and extends in depth in the bigger grain

+ Difference in the peak position for the two systems (agreement with the experimental observations)
+ Relative amplitude difference between the two sizes
+ The trends are reproducible irrespective of the choice of intra and intergrain coefficients

Simulation

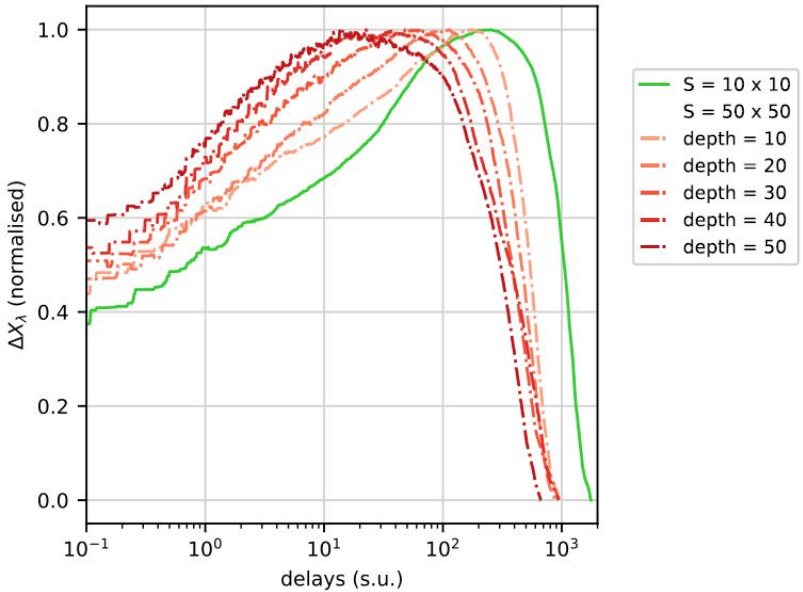

Domains expanding beyond laser penetration allows us to ***reproduce both the time shift and relative amplitude*** observed experimentally

Phase separation on surface and extends in depth in the bigger grain

+ Difference in the peak position for the two systems (agreement with the experimental observations)
+ Relative amplitude difference between the two sizes
+ The trends are reproducible irrespective of the choice of intra and intergrain coefficients

Simulation

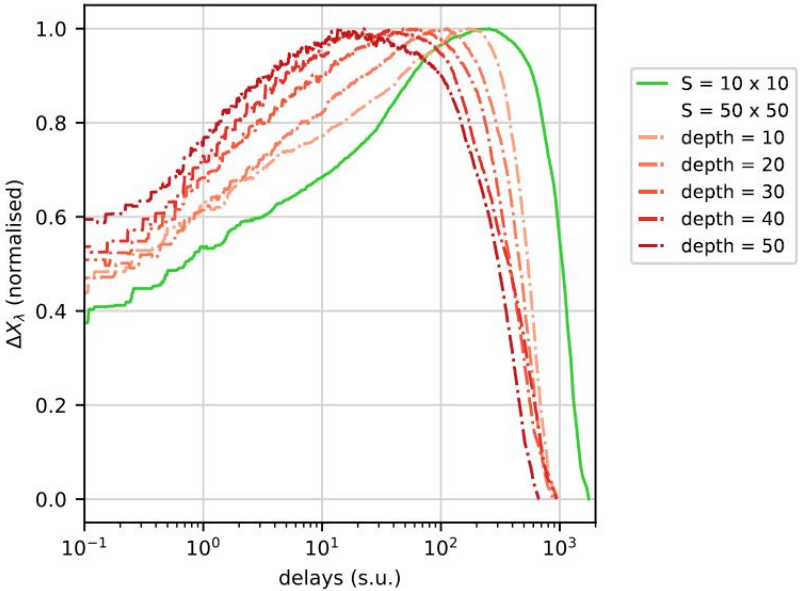

Experiment

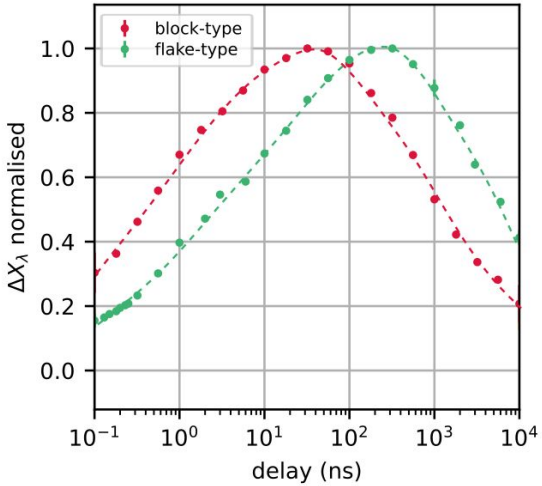

Domains expanding beyond laser penetration allows us to ***reproduce both the time shift and relative amplitude*** observed experimentally

Conclusion

- The phase transition due to heat diffusion reaches a maximum peak at the ns timescales.
- This peak position depend on the grainsize of the pellets.

- The transition due to heat diffusion reaches maximum at an early delay in the bigger crystallites compared to the smaller crystallites.

- This counterintuitive peak shift and the relative amplitude between the grain sizes have been reproduced successfully by the model, with phase separated domains extending beyond the laser penetration depth

Simulation

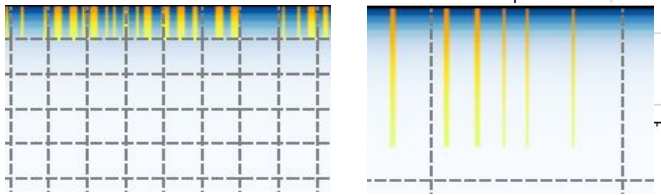

Experiment

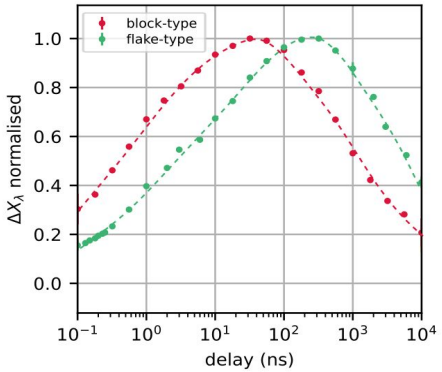

Future prospects

Time resolved electron diffraction on individual nanocrystals

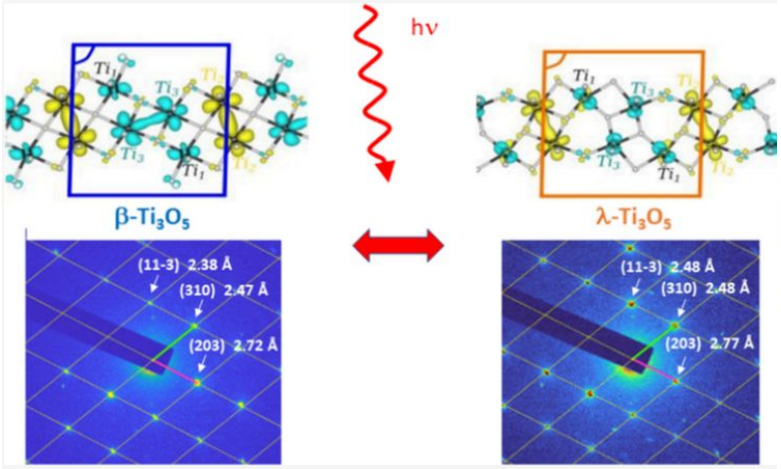

The Journal of Physical Chemistry C

C: PHYSICAL PROPERTIES OF MATERIALS AND INTERFACES | August 7, 2024

Phase Transformations of Individual Ti_3O_5 Nanocrystals Studied by *In Situ* Electron Microscopy

Yaowei Hu, Hilaire Mba, Matthieu Picher, Hiroko Tokoro*, Shin-ichi Ohkoshi, Céline Mariette, Ritwika Mandal, Maryam Alashoor, Philippe Rabiller*, Maciej Lorenc, and Florian Banhart*

Future prospects

Lamella shaped single crystals extracted from the bulk crystals using FIB technique.

Study strain propagation in a single object along different crystallographic axes

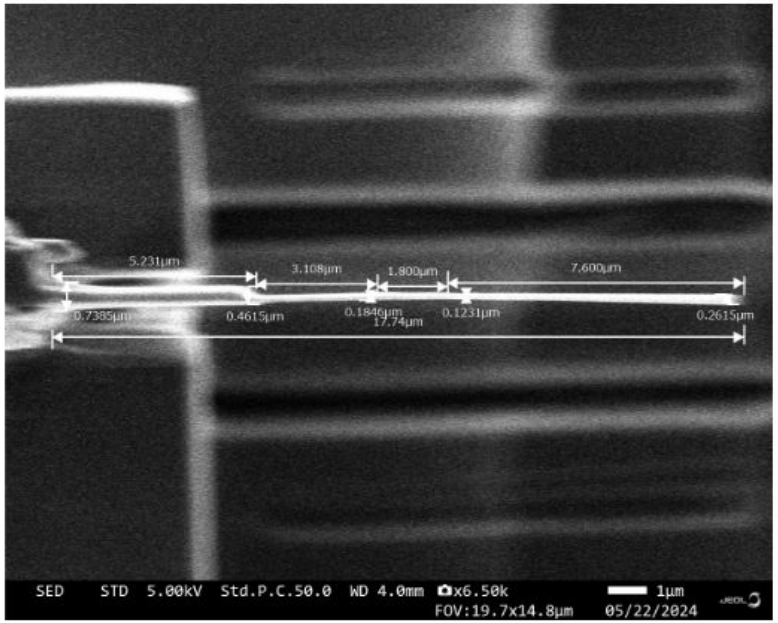

(Rennes, France)
Maciej LORENC
Bruno LEPINE
Elzbieta TRZOP
Herve CAILLEAU

(ID09 beamline, Grenoble, France)
Céline MARIETTE
Matteo LEVANTINO
Marco CAMMARATA
Serhane ZERDANE

Alexandru Ioan Cuza University of Iasi
(Iasi, Romania)
Laurentiu STOLERIU
Christian ENACHESCU

(Japan)
Shin-ichi OHKOSHI

(Japan)
Hiroko TOKORO
Marie YOSHIKIYO

(Nantes, France)
Etienne JANOD
Laurent CARIO

Thank you for your attention

Appendix

Spatial laser and X-ray overlap in Ti_3O_5 pellets

- The three polycrystalline powder was pressed to form pellets of 8 mm in diameter
- AFM study shows the pellets have a surface roughness of 350 nm

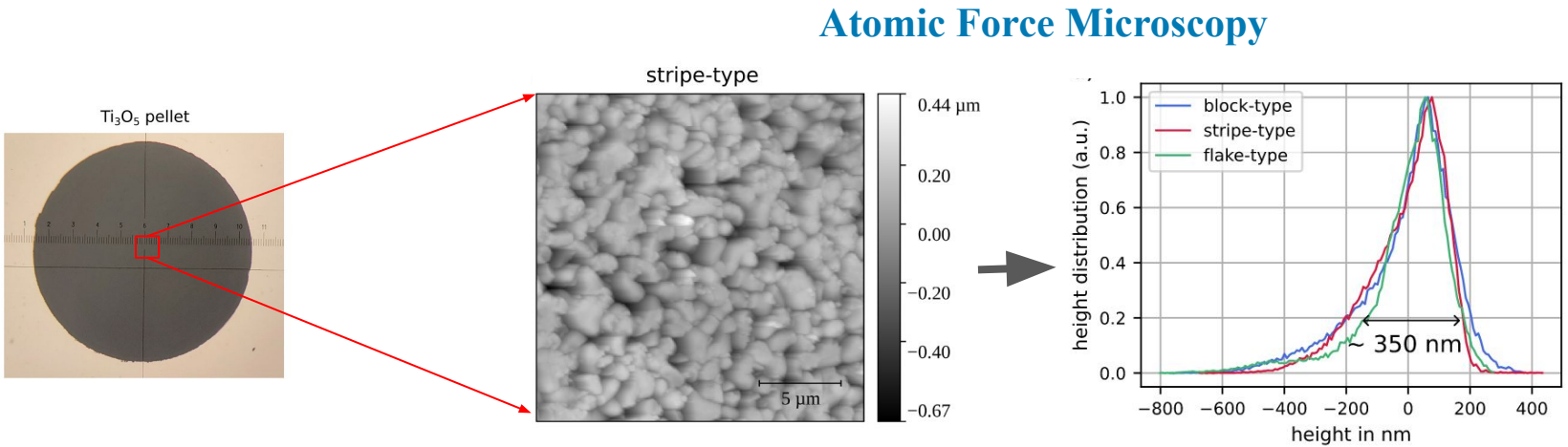

- Laser penetration depth ~ **70 nm** (for 800 nm wavelength)
  ~ **140 nm** (for 1550 nm wavelength)

- X-ray penetration depth ~ 450 nm at 0.4^0 incidence angle
  Effective penetration depth ~ **800 nm**

Results and observation from the comparison plots:

Influence of incident laser fluence on the phase transition dynamics

Linear dependence on the laser fluence at 200 ps (transformed by strainwave)
Non-linear dependence with fluence at 100 ns (transformed by heat diffusion)

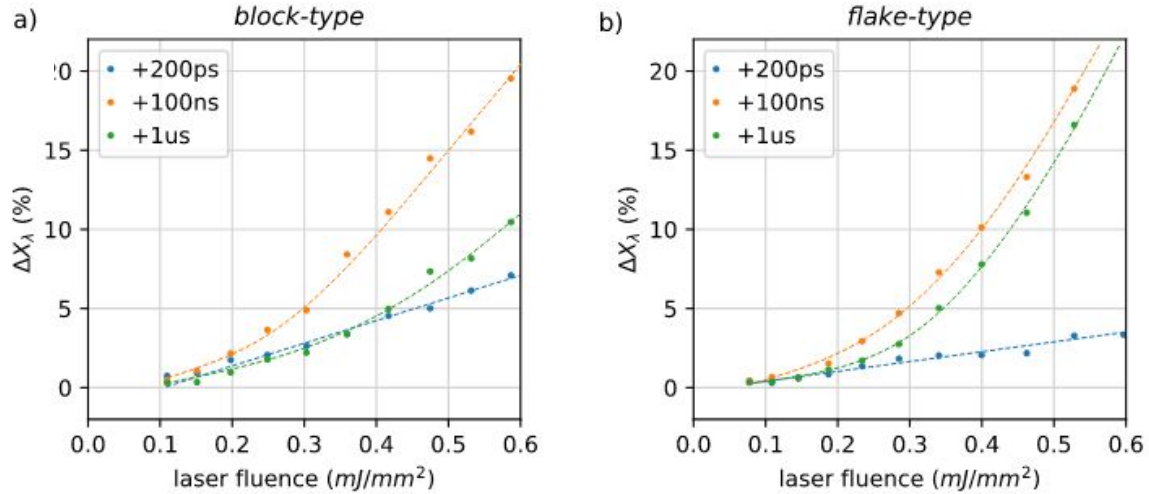

Different fluence dependencies confirm the ***different mechanism at play on 200 ps and 100 ns time scales***

Results and observation from the comparison plots:

Influence of incident laser pump wavelength on the phase transition dynamics

Other parameters are kept same:

- laser fluence = 0.5 mJ/mm^2
- Incidence angle of x-ray beam = 0.4°
- Laser penetration depth
  ~ **70 nm** (for 800 nm wavelength)
  ~ **140 nm** (for 1550 nm wavelength)

Peak of the ΔX_λ occurs at the same delay irrespective of the photon energy

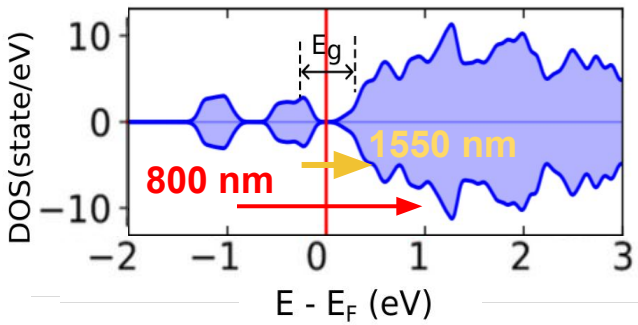

500 nm crystallites | **100 nm crystallites**

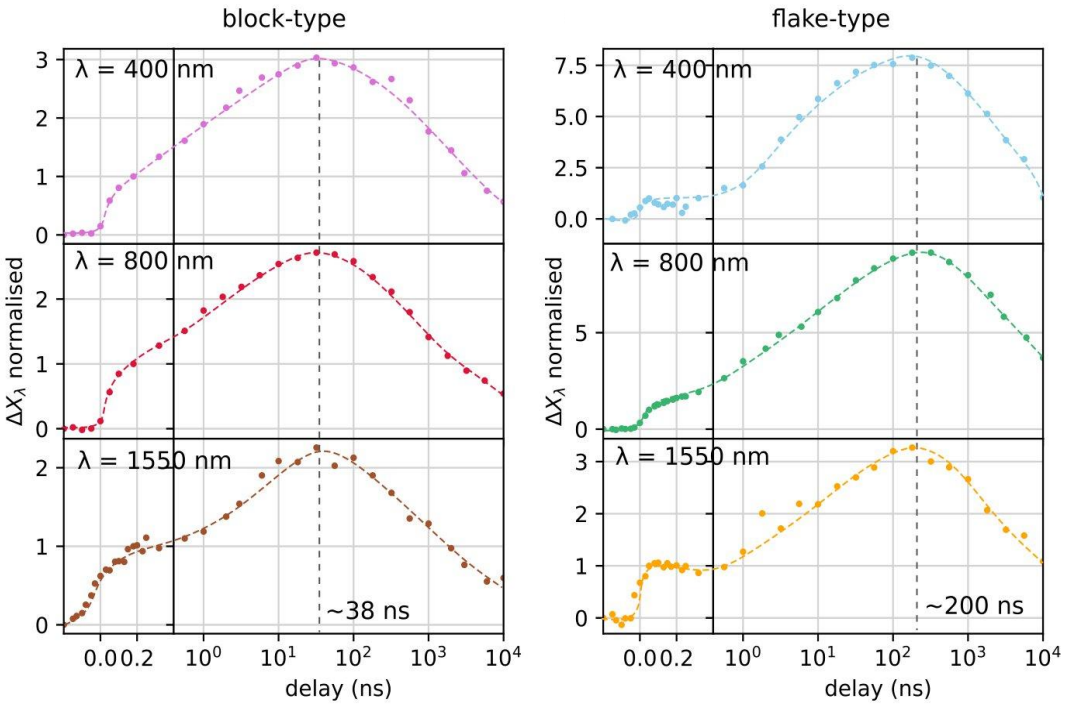

The position in time of the heat diffusion peak does not depend on pump wavelength and pump penetration.

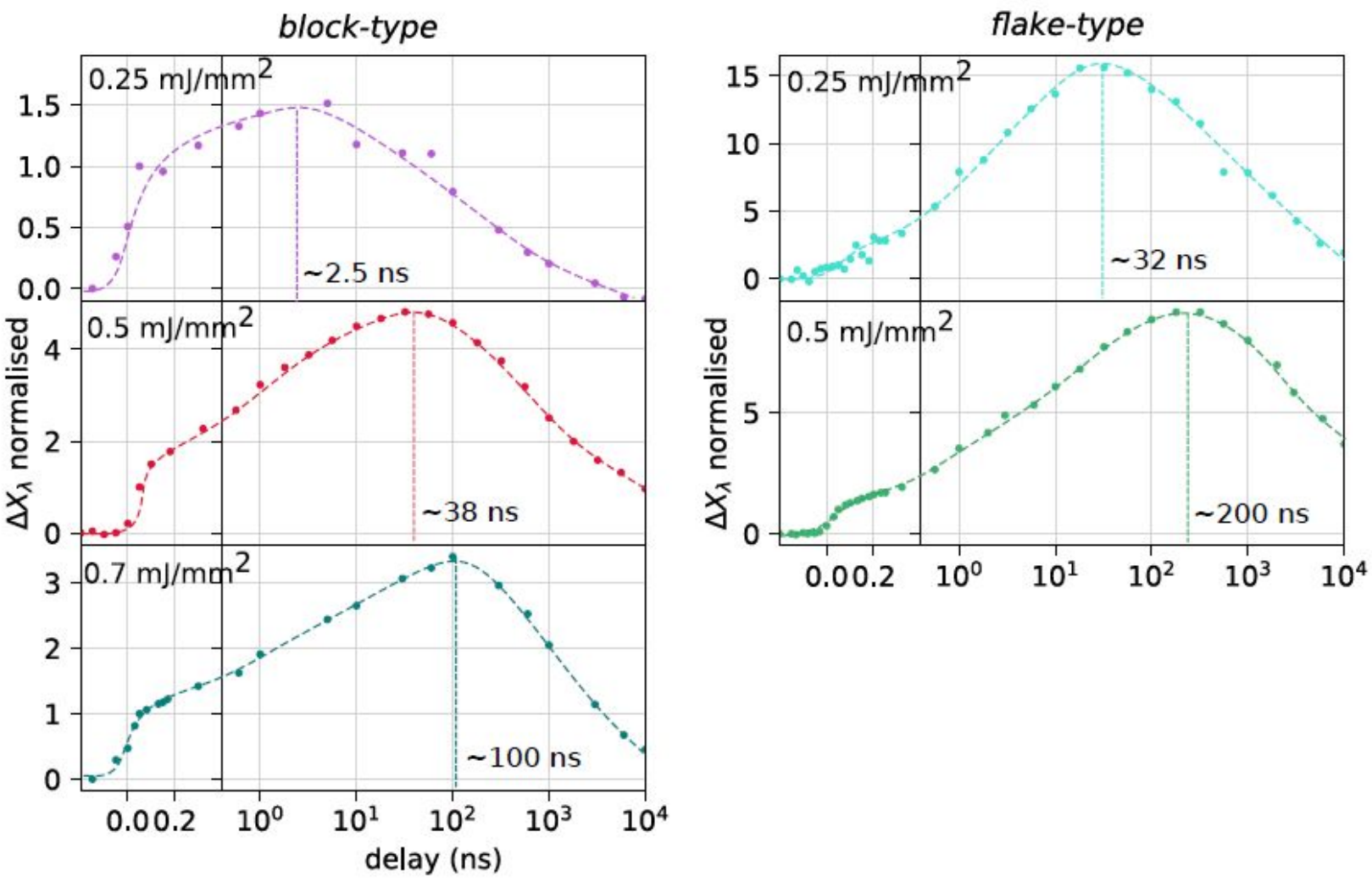
block-type
flake-type
0.25 mJ/mm2
0.5 mJ/mm2
0.7 mJ/mm2
~2.5 ns
~38 ns
~100 ns
~32 ns
~200 ns
ΔXλ normalised
delay (ns)

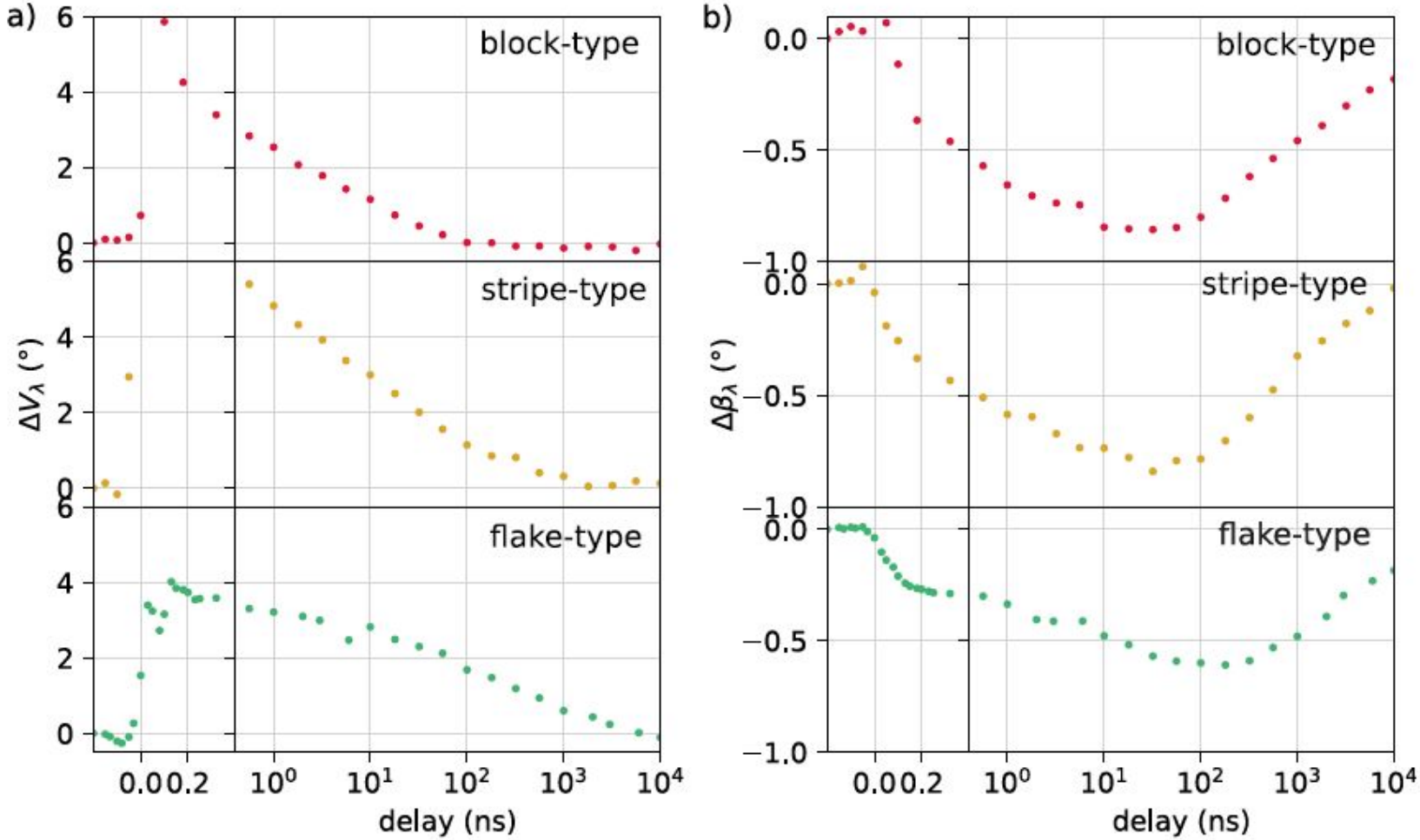
a)
b)
block-type
stripe-type
flake-type
ΔV_λ (°)
$\Delta\beta_\lambda$ (°)
delay (ns)
0.0 0.2
10^0
10^1
10^2
10^3
10^4

Domains on photoexcited surface limited in depth by laser penetration depth

Initial state: λ-phase domains that are

1. Over the whole photoexcited crystallite
2. Limited in depth by laser penetration

Grainsize: 10x10

Grainsize: 20x20

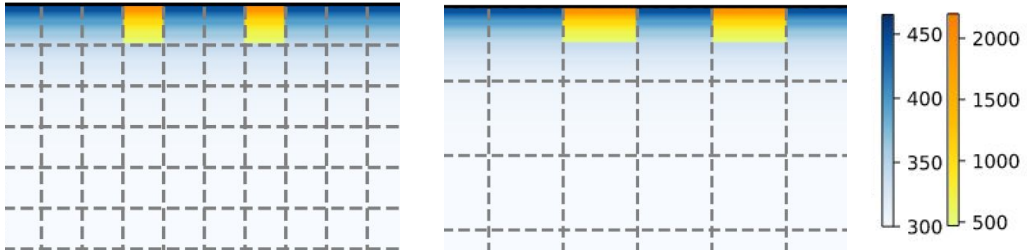

- Difference in the peak position for the two systems; in opposite trend to the experimental results(Irrespective of the inter- and intra-grain coefficients)

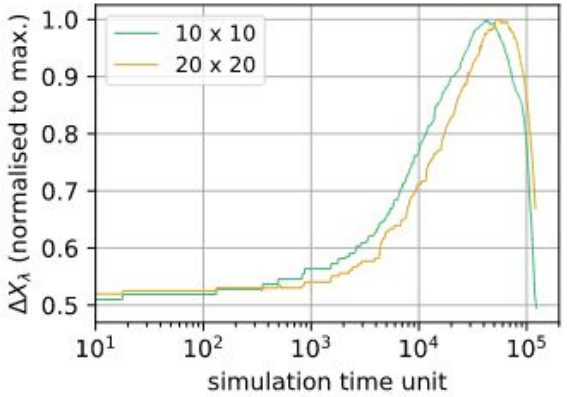

Domains which are photoexcited on the surface but limited in depth by the laser penetration depth cannot explain the size dependance in the ns dynamics.

Phase separation on surface and limited in depth by laser penetration

Initial state: λ-phase domains that show
1. phase separation within a crystallite
2. Limited in depth by laser penetration

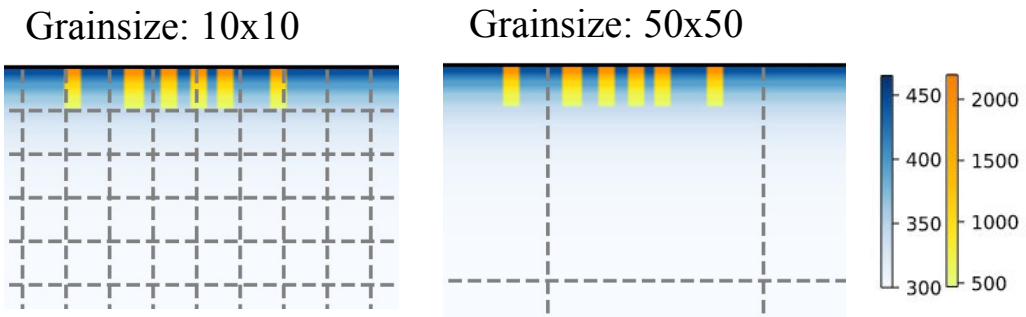

\+ Difference in the peak position for the two systems (agreement with the experimental observations)

\- During the rising time, no difference in the relative amplitude

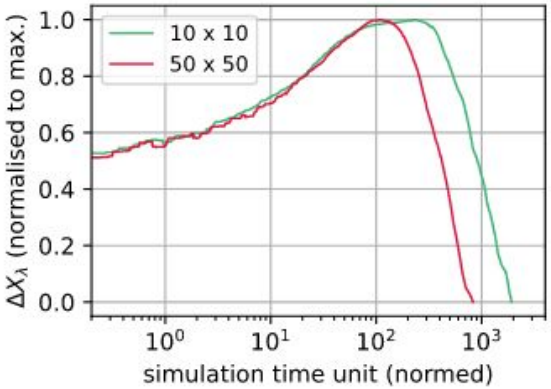

Phase separation within crystallites and along the surface allows us to reproduce the time shift observed experimentally

Discussion on the model hypothesis and parameters

- ***Exponentially decreasing temperature*** from a surface temperature of 2500 K
- The temperature was estimated from the incident laser power and reflectivity of the pellet
- The thermal exchange coefficients were estimated from the thermal conductivity values of λ and β phases of Ti_3O_5 and air.

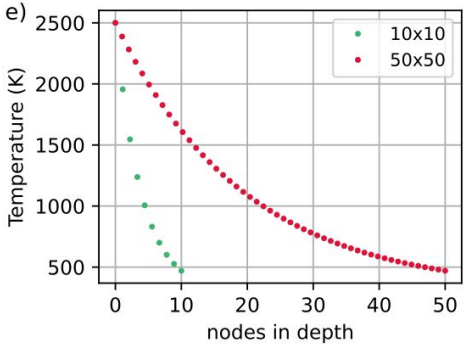

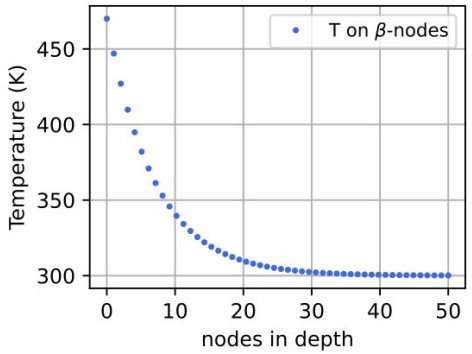

coefficient	simulation value	value from thermal conductivities (WK^{-1})
$c_{i,i}^{\lambda\lambda}$	1e-2	2e-9
$c_{i,i}^{\beta\beta}$	2e-2	4e-9
$c_{i,i}^{\beta\lambda}$	1.35e-2	2.7e-9
$c_{i,j}^{\lambda\lambda}$	1e-3	2e-10
$c_{i,bulk}^{\beta}$	1e-5	4.2e-14
$c_{i,air}^{\beta}$	1e-8	2.5e-15